Issue 1

CUTTING EDGE

Glaucoma

Access the contents & video on the online portal:

http://collections.medengine.com/ophthalmology/cutting-edge-glaucoma/

Springer Healthcare Education

SUN PHARMA

SOME HEIGHTS ARE THRILLING

BUT AN ELEVATED IOP IS NOT

In Glaucoma, 40% of treated patients required two or more medications to achieve a 20% reduction from baseline IOP by year 5[1]

In Primary Open Angle Glaucoma & Ocular Hypertension

℞ BRIMOLOL

Brimonidine Tartrate 0.15% + Timolol Maleate 0.5%

For Combined Power, Greater Benefits...

36% (8.3 mmHg) additional IOP reduction from latanoprost treated baseline[1]

At 12 weeks, fixed-dose combination provided 8.3 mmHg IOP reduction from latanoprost baseline at peak effect (~2 mmHg more than adjunctive timolol)[1]

IOP - Intra Ocular Pressure | 1. Clinical Ophthalmology 2011:5 945-953

CUTTING EDGE
Glaucoma

Springer Healthcare Education

March 2022

Springer Healthcare

This edition is published by Springer Nature India Private Limited.
Registered Office: 7th Floor, Vijaya Building, 17, Barakhamba Road, New Delhi 110 001, India.
T: +91 (0) 11 4575 5888
www.springerhealthcare.com

Part of the Springer Nature group

Contents

WHAT'S NEW

CLINICAL VIGNETTE

Videos available online:

Congenital Glaucoma and Anterior Segment Dysgenesis

1. Surgery with buphthalmic eye.
2. Technique of intraoperative gonioscopy in suspected anterior segment dysgenesis.

Step by step procedure for online viewing:

1. Go to http://collections.medengine.com/ophthalmology/cutting-edge-glaucoma/ or scan QR code.
2. Web page of the issue will open on the screen.
3. View and read the PDF version and watch the videos online.
4. The PDF file can be downloaded too for offline reading.

WHAT'S NEW

AI and Glaucoma

Zhiqi Chen, Gadi Wollstein, Joel S. Schuman, Hiroshi Ishikawa

Glaucoma is characterized by progressive loss of retinal ganglion cell (RGC) and their axons which may result in optic nerve head (ONH) and retinal nerve fiber layer (RNFL) changes and eventually lead to vision loss and irreversible blindness [1-3]. Since glaucoma is a slowly progressing disease with irreversible neural damage, early diagnosis and sensitive progression monitoring are essential to glaucoma management. For clinical assessment, structural (e.g. fundus photography (Fig. 1)), optical coherence tomography (OCT, Fig. 2) and functional (e.g. visual field (VF, Fig. 3)) measurements are commonly assessed in addition to the conventional observations (e.g. optic disc assessment, intraocular pressure (IOP)). Various longitudinal studies on glaucoma progression reported contradicting non-linear relationships between structural and functional measurements [4-10]. There are complex, non-linear, asynchronous interactions between them, which have not been fully understood yet.

Recently, artificial intelligence (AI) has started to impact in ophthalmology [11-15]. Deep learning (DL) is a class of state-of-the-art machine learning (ML) algorithms that are especially tailored to extract meaningful features from complex and high-dimensional data. Consequently, AI algorithms, especially DL, have the potential to revolutionize the diagnosis and management of glaucoma based on the interpretation of functional and/or structural information and even to improve the understanding of glaucoma by defining the structural features responsible for certain functional damages and to identify phenotypes that follow similar progression patterns. Table 1 summarizes current DL applications in glaucoma.

Z. Chen
Department of Electrical and Computer Engineering, New York University, Brooklyn, NY, USA

Department of Ophthalmology, NYU Langone Health, New York, NY, USA
e-mail: zc1337@nyu.edu

G. Wollstein · H. Ishikawa (✉)
Department of Ophthalmology, NYU Langone Health, New York, NY, USA

Department of Biomedical Engineering, New York University, Brooklyn, NY, USA
e-mail: Gadi.Wollstein@nyulangone.org; Hiroshi.Ishikawa@nyulangone.org

J. S. Schuman
Department of Electrical and Computer Engineering, New York University, Brooklyn, NY, USA

Department of Ophthalmology, NYU Langone Health, New York, NY, USA

Department of Biomedical Engineering, New York University, Brooklyn, NY, USA
e-mail: Joel.Schuman@nyulangone.org

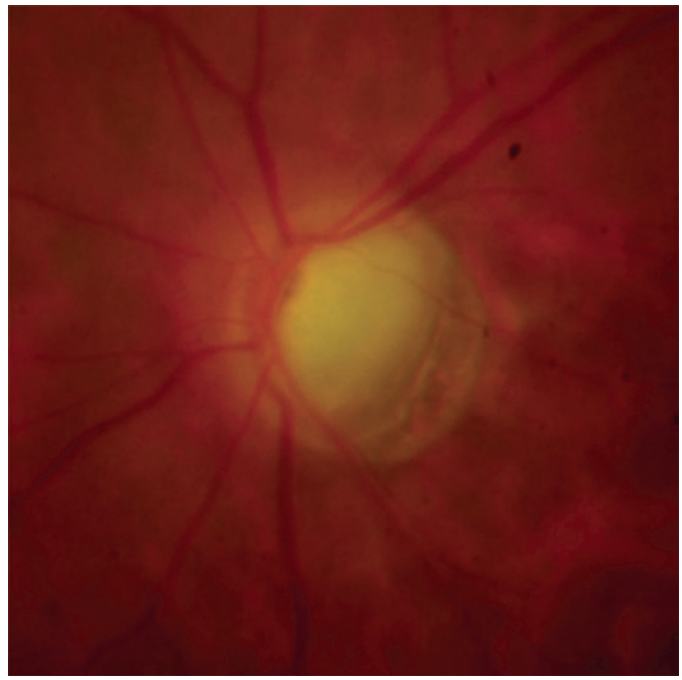

Fig. 1: Fundus photography of a left eye with glaucoma. Large cupping and peripapillary atrophy are shown in the image.

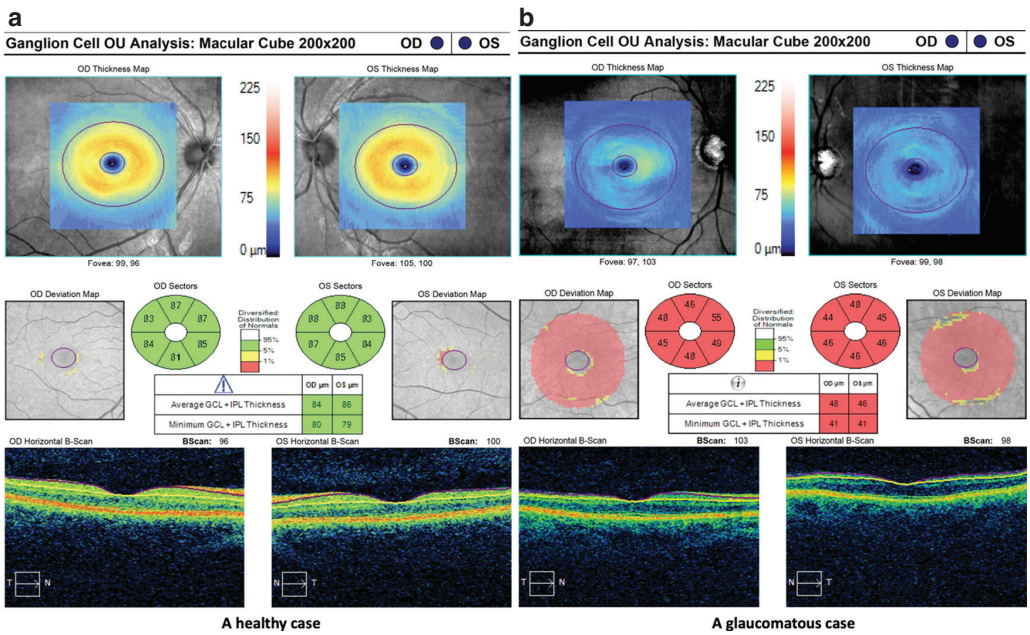

Fig. 2: Examples of Cirrus OCT report from a healthy case (**a**) and a glaucomatous case (**b**). The image is color-coded (red, orange, and yellow represent thicker areas while green and blue represent thinner areas).

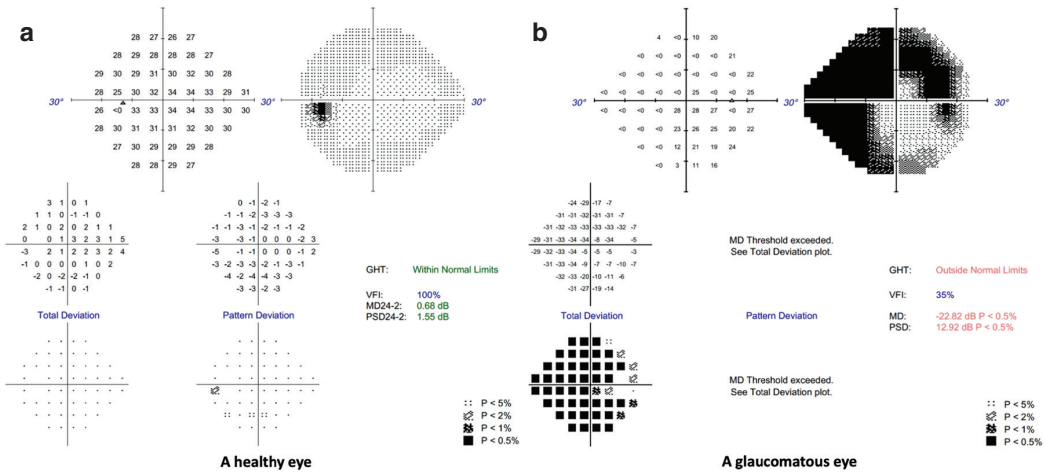

Fig. 3: Examples of Humphrey 24-2 VF report from a healthy eye (**a**) and a glaucomatous eye (**b**). Figure (**b**) shows advanced visual field damages with superior nasal deficit, large inferior nasal step and superior temporal step, and paracentral scotoma.

Table 1: Summary of DL applications in glaucoma.

Application	Subtasks	Data type	Models	References
Glaucoma diagnosis	Segmentation, object detection, classification	Fundus photography, OCT, VF, demographic features, IOP, *et al.*	FNN, CNN, ResNet, Faster RCNN, U-Net	[15–33]
Longitudinal analysis	VF forecasting, structural loss forecasting	VF, RNFL thickness, GCIPL thickness	RNN, CNN, LSTM	[34–36]
Structural-functional relationship discovery	Mapping between structural features and functional measurements (VF thresholds, VFI, VF MD *et al.*)	OCT, retinal thickness map	CNN, ResNet50	[37–41]
Knowledge discovery	Age, gender, or race prediction from OCT images	OCT	CNN	[42]
Image enhancement	Speckle noise reduction on OCT images	OCT	GAN	[43]

In this chapter, we provide an overview of current AI applications and challenges in glaucoma. Section "Glaucoma Diagnosis" introduces AI utilization in detecting glaucoma; section "Longitudinal Analysis" focuses on role of AI in longitudinal projection; section "Structural-Functional Correlation" summarizes developments of AI in finding the structural-functional relationship; finally, section "Other AI Applications in Glaucoma" presents some other applications of AI in glaucoma.

Glaucoma Diagnosis

Diagnosis of glaucoma can be modeled as a classification problem which typically has one or multiple features (clinical parameters or images) as input and a single diagnostic variable as output (e.g., presence or severity of glaucoma). It is one of the first areas in which AI is extensively explored.

In 1994, ML classifiers were first used to discriminate normal and glaucomatous eyes based on visual fields [1]. Subsequent studies explored the classification problem with more ML methods and data modalities and demonstrated the effectiveness of ML models. The community initially focused on taking clinical parameters as input and using classical ML classifiers such as random forest (RF) and support vector machine (SVM) and manually designed features for the task, which are problem-dependent and require domain knowledge.

Since 2013, the development of DL, especially convolutional neural networks (CNNs), has enabled automatic learning of discriminative representations of data that optimally solves the problem [44-47]. DL models utilize multiple processing layers to obtain scalability and learn hierarchical feature representations of data with multiple levels of abstraction which are suitable for classification. Therefore, DL models have been studied to improve the accuracy of automated glaucoma diagnosis, summarized in Table 2.

Functional Defects as Input

In clinical practice, VF testing is widely used as the gold standard for disease diagnose and glaucomatous damage assessment. Several classical ML classifiers (i.e., multilayer perceptron (MLP), SVM, and linear (LDA) and quadratic discriminant analysis (QDA), Parzen window and mixture of Gaussian (MOG)) have been proposed to automatically discriminate between normal eyes and eyes with pre-perimetric glaucoma based on visual fields and have shown promising performance [48-50]. With the development of computational capacity, deeper models have become possible to be implemented. Asaoka *et al.* [26] proposed a multi-layer feed-forward neural network (FNN) with stacked denoising autoencoder to classify pre-perimetric glaucoma VFs and healthy VFs and achieved better performance over shallower ML models.

Previous work showed promising performance in classification of VFs. Yet, these methods treated each VF point as individual features and failed to leverage spatial information within VFs. Spatial Information is useful to discover VF defect pattern and therefore helps glaucoma diagnosis [27]. Thus, incorporating spatial information into ML classifiers may boost the discrimination ability. CNN is an evolution of FNN which replace matrix multiplication with convolution to process spatial information. Thus, researchers started to implement CNN models to discriminate VFs.

Kucur *et al.* [28] converted VFs to images using a Voronoi parcelation [51]. A seven-layer CNN, which explicitly took spatial information into account through spatial convolutions, was used to discriminate between healthy and early glaucomatous VFs with those converted images as input. Results demonstrated supremacy of CNN over NN that did not consider spatial information

Table 2: Summary of recent DL work on glaucoma diagnosis.

Input type	Reference	Models	Subtasks	Input data	Output classes
Functional	[26]	FNN	Classification	Individual VF thresholds	Glaucoma/ non-glaucoma
	[28]	CNN	Classification	VF map	Early glaucoma/ non-glaucoma
	[29]	CNN	Classification	Probability map of VF PD	Glaucoma/ non-glaucoma
Structural	[21]	CNN	Classification	Color fundus image	Glaucoma/ non-glaucoma
	[15]	CNN	Classification	Color fundus image	Glaucoma/ non-glaucoma
	[22]	Hierarchical ResNet, UNet	Classification	Color fundus image	Glaucoma/ non-glaucoma
	[23]	Inception-v3	Classification	Color fundus image	Glaucoma/ non-glaucoma
	[24]	CNN	Classification	Color fundus image	Glaucoma/ non-glaucoma
	[30]	CNN, Random forest	Feature extraction, classification	RNFL thickness map, GCIPL thickness map, RNFL probability map, GCIPL probability map, and en face projection image	Glaucoma/ non-glaucoma
	[31]	Multi-Context Deep Network	Classification	2D Anterior Segment OCT image	Open-angle/ angle-closure glaucoma
	[32]	3D CNN	Classification	3D OCT volume	Glaucoma/ non-glaucoma
	[33]	CNN	Classification	RNFL probability map	Glaucoma/ non-glaucoma
Mixed	[25]	CNN, Faster-RCNN, FCN	Feature extraction, OD region detection, OC segmentation, classification	Color fundus image, age, IOP, eyesight, and symptoms	Glaucoma/ non-glaucoma

(average precision score: 0.874 ± 0.095 vs. 0.843 ± 0.089). By computing the gradient, saliency maps can be obtained to visualize important pixels that contribute most to the outputs of CNN. The saliency maps suggested that CNNs were capable of detecting patterns of localized VF defects.

Li *et al.* [29] took probability map of pattern deviation (PD) from the VF reports as the input to a CNN. Results showed that CNN achieved higher accuracy compared to ophthalmologists, rule-based method (Advanced Glaucoma Intervention Study (AGIS) criteria and Glaucoma Staging System (GSS) criteria), and traditional machine learning algorithms (SVM, RF, k-nearest neighbor).

Structural Damages as Input

Assessment of structural damage has become a practical standard for glaucoma diagnosis. Early studies focused on structural measurements obtained from imaging techniques such as confocal scanning laser ophthalmoscopy (CSLO) and scanning laser polarimetry (SLP) [47, 52-58]. Promising performance of ML classifiers on structural parameters such as optic disc parameters measured by CSLO and RNFL measurements from SLP were reported. However, due to the popularity of the technologies, recent AI-based studies on structural glaucomatous damages have focused on fundus photography and OCT.

Fundus Photography

Fundus photography is a well-established and cost-effective imaging technique to identify features of the fundus region including fovea, macula, optic disc (OD), and optic cup (OC). Glaucoma can be identified by the optic nerve cupping. Thus cup-to-disc ratio (CDR), which measures the vertical diameter of the optic cup to that of the disc, is one of the most important biomarkers for glaucoma diagnosis. Higher CDR value indicates a higher probability of glaucoma. Therefore, many AI-based studies focused on automatic segmentation of OD and OC using deep learning [16-21]. Segmentation-based methods, however, lack sufficiently discriminative representations and are easily affected by noise and low image quality. Moreover, predefined clinical parameters lack complex morphological information that might be useful in the diagnosis. Therefore, more recent methods simultaneously learn discriminative representation that optimize classification results directly from fundus images.

In 2015, Chen *et al.* [15] proposed a six-layer CNN to classify glaucoma and non-glaucoma eyes directly from fundus images from public available ORIGA dataset [59] and SCES dataset [60]. Experimental results showed AUC of 0.831 and 0.887 on ORIGA and SCES respectively. In a later work, Chen *et al.* [61] designed a novel CNN which embed multilayer perceptron to discriminate glaucoma and non-glaucoma patterns of fundus images.

In 2018, Fu *et al.* [22] proposed a Disc-aware Ensemble Network (DENet) which consisted of four streams to integrate hierarchical context of global fundus images and local OD regions. The first stream used a Residual Network (ResNet) [62] to learn the global representation on the whole fundus image directly and produce a glaucoma classification probability. The second stream adapted the U-shape CNN (U-Net) [63], which is an efficient DL model for medical image segmentation, to produce the disc probability map and a glaucoma classification probability. The third stream cropped OD region image as input and output a classification probability through a ResNet. The fourth stream applied the pixel-wise polar transformation to transfer the copped original image to the polar coordinate system in order to enlarge the cup region and augment data. Then, a ResNet was trained to output a classification probability. The model was trained on ORIGA dataset and yielded testing results of an accuracy of 0.832 on SCES and 0.666 on SINDI datasets.

Later, Li *et al.* [23] applied Inception-v3 [64] on a private dataset to detect referable glaucomatous optic neuropathy (GON) and achieved an AUC OD 0.986 with sensitivity of 0.956 and specificity of 0.92. Results also showed that other eye conditions would greatly affect the detection accuracy. High or pathological myopia contributed most to false-negative results while physiologic cupping and pathological myopia are the most common reason for false-positive results.

Though previous methods demonstrated the efficiency of DL in glaucoma diagnosis, DL methods suffer from overfitting problem due to relatively small dataset available and a large number of parameters needed training. In 2018, Chakravarty *et al.* [24] presented a multi-task CNN that segmented OD and OC on fundus images and jointly classified the image to glaucoma and non-glaucoma. The proposed method was evaluated on the REFUGE dataset to achieve an average dice score (which measures the overlap of segmentations and ground truths) of 0.92 for OD segmentation, 0.84 for OC segmentation, and AUC of 0.95 for classification. The cross-task design reduced the number of parameters and ensured good generalization of the model on small dataset. In another work, Chai *et al.* [25] designed a multi-branch neural network (MB-NN) model to leverage domain knowledge includes important measures (e.g., CDR) for glaucoma diagnosis. The first branch extracted hidden features directly from fundus image through a CNN. The second branch used Faster-RCNN [65] which is a deep learning framework for object detection to obtain optic disc region. Then another CNN is used to extract local hidden features. The third branch used a fully convolutional network (FCN) [66] to segment OD, OC, and peripapillary atrophy (PPA), and then calculated measures related to disc, cup, and PPA. RNFL defects, a roughly wedge shape region starting from OD, detected from another CNN and non-image features (e.g. age, IOP, eyesight and symptoms) from case reports were also inputs to the third branch. The proposed framework was verified on a private dataset and achieved an accuracy of 0.915, sensitivity of 0.9233, and specificity of 0.909.

OCT

OCT, which is a non-invasive imaging technique to provide micrometer resolution cross-sectional and volumetric images of retina, has emerged as the de facto standard in objective quantification of structural damage in glaucoma. Similarly, early studies focused on comparison of various classical ML classifiers using parameters measured by OCT [67-69]. Though classical ML classifiers classified glaucoma with satisfying accuracy, the limitation of ML classifiers is the reliance of the segmentation of retinal layers that uses handcrafted features and is prone to errors. Therefore, deeper and segmentation-free methods were desired to avoid the problem.

In 2017, Muhammad *et al.* [30] used a pre-trained CNN model for feature extraction and a random forest model for classification. Though the proposed model is deep, the images fed into the model were still generated by conventional segmentation methods: (1) retinal ganglion cell plus inner plexiform layer (GCIPL) thickness map; (2) RNFL thickness map; (3) GCIPL probability map; (4) RNFL probability map; (5) en face projection. The results showed that the proposed method with the RNFL probability map as input outperformed OCT and VF clinic but fell short of an experienced human expert.

In 2018, Fu *et al.* [31] present a Multi-Context Deep Network (MCDN) to classify angle-closure and open-angle glaucoma based on Anterior Segment Optical Coherence Tomography (AS-OCT). The anterior chamber angle (ACA) region was first localized by a data-driven AS-OCT structure segmentation method [22] to compute the clinical parameters (e.g., Anterior Chamber Width, Lens-Vault, Chamber Height, Iris Curvature, and Anterior Chamber Area). A linear SVM was employed to predict an angle-closure probability based on these clinical parameters. Then localized ACA region and the original scan were fed into two parallel CNNs to jointly gain local and global discriminative representations respectively and output an angle-closure probability. Finally, the probabilities from clinical parameters and CNNs are averaged to produce the final results. Experimental results showed that the proposed method is effective for angle-closure glaucoma screening. Detailed analysis of three input streams showed that DL-based global discriminative features did not work as well as handcrafted visual features (AUC 0.894 vs. 0.924) while DL-based local discriminative features achieved on par performance with handcrafted features (AUC 0.920 vs. 0.924).

In 2019, Maetschke *et al.* [32] proposed a 3D CNN to be trained directly on raw spectral domain optical coherence tomography (SD-OCT) volumes of ONH to classify healthy and glaucomatous eyes. The class activation map (CAM) analysis found neuroretinal rim, optic disc cupping, and lamina cribrosa and its surrounding area were significantly associated with the classification results, which aligned with commonly used clinical markers for glaucoma diagnosis such as neuroretinal thinning at the superior and inferior segments and increased cup volume.

In the same year, RNFL probability maps, which are generated based on swept-source optic coherence tomography (SS-OCT) to superimpose structural changes with VF locations, were also trained with CNNs to discriminate between glaucomatous and healthy eyes [33]. CAM analysis suggested that anatomical variation in blood vessel or RNFL location caused ambiguity in false positive and false negative. This discovery might be useful for future improvement of DL systems by supplying information about blood vessels.

Combining Structure and Function

Many studies also developed effective ML classifiers combining structural and functional data. Global VF indices (mean defect, corrected loss variance, and short-term fluctuation) in combination with structural data (CDR, rim area, cup volume, and nerve fiber layer height) analyzed by an ANN was capable to correctly identify glaucomatous eyes with an accuracy of 88% in an early study [70]. This figure was higher than that of the same ANN trained with only structural or functional data. The development of computational ability accommodated larger models and larger inputs. Bowd *et al.* [71] took complete VF maps and OCT RNFL thickness measurements of 32 sectors to train multiple ML learning classifiers. In a later study, Silva *et al.* [24] tested several classifiers, including bagging (BAG), naïve bayes (NB), MLP, radial basis function (RBF), RF, ensemble selection (ENS), classification tree (CTREE), ada boost M1 (ADA), SVM, using 17 RNFL thickness parameters (average thickness, 4 quadrants and 12 clock hour measurements) and mean deviation (MD), pattern standard deviation (PSD), and glaucoma hemifield test (GHT). RF achieved the best AUC result of 0.946.

Generally speaking, DL models are capable of learning discriminative representations and identifying glaucoma patients. However, comparing those methods remains challenging because of the variety of training and testing datasets and validation methods. The possibility to extract knowledge that might not be discovered before, such as unknown glaucoma related structures/features that are highly associated with glaucomatous damages and glaucoma phenotyping, is the most exciting part of DL. Therefore, increasing interpretability of DL to visualize learned knowledge will be critical to future development of the use of DL in glaucoma diagnosis.

Longitudinal Analysis

The accelerated retinal ganglion cell loss is a characteristic feature of glaucoma progression together with functional damages. Therefore, identifying progression and estimating the rate of loss either structurally or functionally are crucial to glaucoma management.

The current clinical gold standard for progression analysis is the Guided Progression Analysis (GPA) provided by the commercial software developed by Carl Zeiss [72, 73]. The software allows clinicians to evaluate the patient's functional or structural loss over time compared to his or her own baseline, which is a composite of two initial examinations. Event-based and trend-based analysis are two approaches to tell whether the progression exists. Event-based analysis evaluates changes from baseline compared to expected variability. The expected variability is determined by the 95% confidence intervals of the magnitude of fluctuation of stable glaucoma patients from empirical datasets. Progression is defined as the change exceeds the expected variability. Trend-based analysis estimated the rate of change over time using linear regression. While GPA is useful to define and quantify glaucoma progression, GPA does not forecast future progressions, which could augment clinical decision making.

For VF forecasting, Caprioli *et al.* [74] projected individual VFs through an exponential model which characterized fast or slow progression rate in VF losses better than linear models. However, both linear model and exponential model assume constant loss rates of VF loss, which usually decay over time [75]. To better depict glaucomatous damage, Chen *et al.* [76] compared pointwise linear, exponential, logistic functions, and combinations of functions and showed that a combination of exponential and logistic functions predicted future progressions better. Previous methods treated test points as individual points and did not incorporate spatial correlations between VF test points at the time point. Several statistical methods have been proposed to incorporate spatio-temporal correlations in VFs [77-80].

Application of DL in this field of predictive medicine is particularly interesting to management of glaucoma since many factors contributing to the rate or severity of glaucoma progression still remain unknown. But unlike the more definitive diagnosis of glaucoma, there have been limited investigation into the potential of DL in predicting future findings. Park *et al.* [34] developed a recurrent neural network (RNN) to predict the sixth visual field test. The performance of RNN was compared with that of a point-wise linear regression. Results showed that VFs predicted by RNN were more accurate than that by linear regression (root mean square error (RMSE): 4.31 ± 2.54 dB vs. 4.96 ± 2.76 dB, $p < 0.001$) and RNN was more robust (smaller and more slowly

increasing of RMSE as the false negative rate increases). However, the proposed method required a large number of VF tests over a long period of time. And many years of VF testing would be needed to accurately predict the future VFs. To overcome the problem, Wen *et al.* [81] trained a deep learning model on the temporal history for a large group of patients to accurately predict future VFs up to 5.5 years given only a single VF test, with a correlation of 0.92 between MD on predicted VFs and MD on actual future VFs.

For structural progression forecasting, Song *et al.* [82] proposed a 2D continuous-time hidden markov model to predict average circumpapillary RNFL thickness and VFI. Sedai *et al.* [35] developed a ML regressor to forecast circumpapillary RNFL thickness at the next visit from multimodal data including clinical (age and IOP), structural (circumpapillary RNFL thickness derived from OCT scans and DL-extracted OCT features), and functional (VF parameters) data of three prior visits and the inter-visit intervals. Chen *et al.* [36] also investigated the predictive DL in predicting structural loss. A time-aware long short-term memory network was designed to predict fifth visit of GCIPL thickness map based on four prior maps and took uneven intervals between every two visits into account.

Structural-Functional Correlation

Relationships between structural loss and functional loss has been a controversial topic which we still do not have a general consensus yet. Early work has investigated classical ML models such as LR [83], a Bayesian framework with a radial basis function [84], and Bayesian LR [85], and logarithmic regression [86] that map function from structure. However, model performance has been limited and highly depending on assumptions of linear relationship or the gaussian distribution of variability in VF measurements, which is not optimal given that it is usually heavily tailed. Given the success of DL in identifying and forecasting glaucoma, DL may help to improve the understanding of the structural-functional relationship in glaucoma. In addition, VF tests are subjective, time-consuming, and very noisy. Thus, estimating VF from OCT accurately may help to reduce unnecessary VF testing in eyes that are estimated to be stable.

In 2017, Uesaka *et al.* [37] proposed two methods to estimate full-resolution 10-2 mode VF maps from retinal thickness (RT) data including GCIPL thickness maps, RNFL thickness maps and RCL thickness maps. The proposed two methods were affine structured non-negative matrix factorization (ASNMF) and a CNN. Results showed that ASNMF worked better for small data size while CNN was powerful for large data size. 7.27 dB of average root mean squared errors (RMSE) was achieved by ASNMF and 6.79 dB by CNNs.

Later in 2018, Sugiura *et al.* [38] reduced the overfitting effect of CNNs by pattern-based regularization (PBR) which utilized characteristic pattern obtained from a large amount of non-paired VF-RT data. Characteristic VF patterns were extracted with an unsupervised learning method. Then, the model was regularized by adding a regularization term to the loss function. The regularization term penalizes the model if the estimation is far from the manifold formed by the extracted VF patterns. Moreover, the location-wise estimation at the last layer of CNNs was replaced by group-wise estimation to reduce network parameters. VF locations were first

categorized into several groups depending on functional similarity. Then, an estimation model was shared within each group. 6.16 dB of RMSE was achieved by the model.

In 2019, Christopher *et al.* [39] applied ResNet50 to detect eyes with glaucomatous visual field damage (GVFD) and predict VF MD, PSD, and mean VF sectoral PD from RNFL thickness map, RNFL en face image, and CSLO images. Model parameters were initialized by a transfer learning that trained the model on ImageNet which is a large image recognition dataset and fine-tuned on a private training dataset in order to reduce overfitting effect.

Previous work relied on segmentation-based features which are prone to errors especially with advanced glaucoma and other co-existing ocular pathologies. Segmentation-free DL methods have also been explored. In 2019, Maetschke *et al.* [40] inferred VFI and MD directly from OCT volumes of the ONH or the macula to eliminate the need for layer segmentation. The proposed 3D CNN was compared with several classical ML methods with segmentation-based OCT features and proved to outperform those ML methods. In 2020, Christopher *et al.* [41] used U-Net to predict full-resolution 24-2 and 10-2 mode VF maps from unsegmented SD-OCT circle scans. The R2 of the predicted results ranged from 0.07 dB to 0.71 for 24-2 mode and from 0.01 to 0.85 for 10-2 mode.

Other AI Applications in Glaucoma

One application of AI is to discover new knowledge in glaucoma. Mendoza *et al.* [42] developed a DL method to predict age, sex, and race based on Spectralis OCT RNFL circle scans from healthy individuals, glaucoma suspect, and glaucoma patients. A MAE (95% CI) of 4.5 years (3.9, 5.2) and a strong (R2 (95% CI)) association of 0.73 between predicted and actual age were achieved for predicting age. AUC (95% CI) of predicting race and sex were 0.96 (0.86, 0.99) and 0.70 (0.57, 0.80), respectively. These results suggest that DL can learn demographic features including age, race, and sex that are not apparent to human observers. The research implied that there are still uncovered knowledge to be discovered in retinal OCT scans.

Another application of AI is to enhance OCT scans. Halupka *et al.* [43] presented a CNN using either mean squared error or a generative adversarial network (GAN) with Wasserstein distance and perceptual similarity to reduce speckle noise of OCT images from both healthy and glaucomatous eyes. The results demonstrated the effectiveness of CNNs to denoising OCT B-scams while preserving structural features of retinal layers. Such denoising methods could be extremely useful in the analysis pipeline and ensure the reliability of the following disease assessment.

Conclusion

In this chapter, we discussed the role of AI in glaucoma. Accurate automated diagnosis and prognosis of glaucoma may assist clinicians to increase efficiency, minimize diagnosis errors, and improve overall quality of glaucoma treatments. With its abilities to extract meaningful information from high dimensional and complex multi-modal data, AI may help to discover new

biomarkers, patterns, or knowledge to improve the current understanding of glaucoma, which could be useful for promoting research and development into new treatments.

There are still several challenges for clinical applications of AI in glaucoma. First, datasets used in many studies are small and collected from homogeneous populations while modern AI systems require very large training dataset and are often subject to numerous variabilities. Tremendous efforts would be required to collect a large and general dataset for glaucoma research. Second, the definition of glaucoma is not clear. Disagreements in the definition of the disease phenotypes often happen between experienced ophthalmologists. Therefore, it is hard to obtain high-quality ground-truth labels. Third, despite many efforts in increasing the interpretability of AI models, AI models are still being considered as "black boxes", which limits its clinical adoption. Thus, it is crucial to develop more visualization tools for AI algorithms. Despite these challenges ahead, AI will likely have positive impact on research and clinical practice in glaucoma.

References

1. Tan O, Chopra V, Lu AT, *et al*. Detection of macular ganglion cell loss in glaucoma by Fourier-domain optical coherence tomography. Ophthalmology. 2009;116(12):2305–2314.e1–e2.
2. Quigley HA, Broman AT. The number of people with glaucoma worldwide in 2010 and 2020. Br J Ophthalmol. 2006;90(3):262–7.
3. Ramulu P. Glaucoma and disability: which tasks are affected, and at what stage of disease? Curr Opin Ophthalmol. 2009;20:92.
4. Hood DC, Tsamis E, Bommakanti NK, Joiner DB, Al-Aswad LA, Blumberg DM, *et al*. Structure-function agreement is better than commonly thought in eyes with early glaucoma. Invest Ophthalmol Vis Sci. 2019;60(13):4241–8.
5. Rao HL, Zangwill LM, Weinreb RN, Leite MT, Sample PA, Medeiros FA. Structure-function relationship in glaucoma using spectral-domain optical coherence tomography. Arch Ophthalmol. 2011;129(7):864–71.
6. Leite MT, Zangwill LM, Weinreb RN, Rao HL, Alencar LM, Medeiros FA. Structure-function relationships using the Cirrus spectral domain optical coherence tomograph and standard automated perimetry. J Glaucoma. 2012;21(1):49.
7. Wollstein G, Kagemann L, Bilonick RA, Ishikawa H, Folio LS, Gabriele ML, *et al*. Retinal nerve fibre layer and visual function loss in glaucoma: the tipping point. Br J Ophthalmol. 2012;96(1):47–52.
8. Malik R, Swanson WH, Garway-Heath DF. Structure–function relationship in glaucoma: past thinking and current concepts. Clin Exp Ophthalmol. 2012;40(4):369–80.
9. Harwerth RS, Wheat JL, Fredette MJ, Anderson DR. Linking structure and function in glaucoma. Prog Retin Eye Res. 2010;29(4):249–71.
10. Garg A, Hood DC, Pensec N, Liebmann JM, Blumberg DM. Macular damage, as determined by structure-function staging, is associated with worse vision-related quality of life in early glaucoma. Am J Ophthalmol. 2018;194:88–94.
11. Taylor P, Kalpathy-Cramer J. Machine learning has arrived! Aaron Lee, MD, MSCI-Seattle, Washington.
12. Rahimy E. Deep learning applications in ophthalmology. Curr Opin Ophthalmol. 2018;29(3):254–60.
13. Ting DSW, Pasquale LR, Peng L, Campbell JP, Lee AY, Raman R, *et al*. Artificial intelligence and deep learning in ophthalmology. Br J Ophthalmol. 2019;103(2):167–75.
14. Gulshan V, Peng L, Coram M, Stumpe MC, Wu D, Narayanaswamy A, *et al*. Development and validation of a deep learning algorithm for detection of diabetic retinopathy in retinal fundus photographs. JAMA. 2016;316(22):2402–10.
15. Chen X, Xu Y, Wong DWK, Wong TY, Liu J. Glaucoma detection based on deep convolutional neural network. In: 2015 37th annual international conference of the IEEE engineering in medicine and biology society (EMBC). IEEE; 2015. p. 715–8.
16. Thakur N, Juneja M. Survey on segmentation and classification approaches of optic cup and optic disc for diagnosis of glaucoma. Biomed Signal Process Control. 2018;42:162–89.

17. Shankaranarayana M, Ram SM, Mitra K, Sivaprakasam K. Joint optic disc and cup segmentation using fully convolutional and adversarial networks. In: Fetal, infant and ophthalmic medical image analysis, vol. 10554. Cham: Springer; 2017. p. 168–76.
18. Zilly J, Buhmann JM, Mahapatra D. Glaucoma detection using entropy sampling and ensemble learning for automatic optic cup and disc segmentation. Comput Med Imaging Graphics. 2017;55:28–41.
19. Sevastopolsky A. Optic disc and cup segmentation methods for glaucoma detection with modification of U-Net convolutional neural network. Pattern Recognit Image Anal. 2017;27(3):618–24.
20. Fu H, Cheng J, Xu Y, Wong DWK, Liu J, Cao X. Joint optic disc and cup segmentation based on multi-label deep network and polar transformation. IEEE Trans Med Imaging. 2018:1–9.
21. Al-Bander B, Zheng Y. Dense fully convolutional segmentation of the optic disc and cup in colour fundus for glaucoma diagnosis. Symmetry. 2018;10(4):87.
22. Fu H, Cheng J, Xu Y, Zhang C, Wong DWK, Liu J, Cao X. Disc-aware ensemble network for glaucoma screening from fundus image. IEEE Trans Med Imaging. 2018;37(11):2493–501.
23. Zhixi L, He Y, Keel S, Meng W, Chang R, He M. Efficacy of a deep learning system for detecting glaucomatous optic neuropathy based on color fundus photographs. Ophthalmology. 2018;125(8):1199–206.
24. Chakravarty A, Sivswamy J. A deep learning based joint segmentation and classification framework for glaucoma assessment in retinal color fundus images. arXiv preprint arXiv:1808.01355.
25. Chai Y, Liu H, Xu J. Glaucoma diagnosis based on both hidden features and domain knowledge through deep learning models. Knowl-Based Syst. 2018;161:147–56.
26. Asaoka R, Murata H, Iwase A, Araie M. Detecting preperimetric glaucoma with standard automated perimetry using a deep learning classifier. Ophthalmology. 2016;123(9):1974–80.
27. Sample PA, Chan K, Boden C, Lee TW, Blumenthal EZ, Weinreb RN, *et al*. Using unsupervised learning with variational bayesian mixture of factor analysis to identify patterns of glaucomatous visual field defects. Invest Ophthalmol Vis Sci. 2004;45(8):2596–605.
28. Kucur ŞS, Holló G, Sznitman R. A deep learning approach to automatic detection of early glaucoma from visual fields. PLoS One. 2018;13(11):e0206081.
29. Li F, Wang Z, Qu G, Song D, Yuan Y, Xu Y, *et al*. Automatic differentiation of Glaucoma visual field from non-glaucoma visual filed using deep convolutional neural network. BMC Med Imaging. 2018;18(1):35.
30. Muhammad H, Fuchs T, De Cuir N, De Moraes C, Blumberg D, Liebmann J, Ritch R, Hood D. Hybrid deep learning on single wide-field optical coherence tomography scans accurately classifies glaucoma suspects. J Glaucoma. 2017;26(12):1086–94.
31. Fu H, Xu Y, Lin S, Wong D, Mani B, Mahesh M, Aung T, Liu J. Multi-context deep network for angle-closure glaucoma screening in anterior segment oct. In: International Conference on Medical Image Computing and Computer-Assisted Intervention. Springer; 2018. p. 356–63.
32. Maetschke S, Antony B, Ishikawa H, Wollstein G, Schuman J, Garnavi R. A feature agnostic approach for glaucoma detection in OCT volumes. PLoS One. 2019;14(7):e0219126.
33. Thakoor KA, Li X, Tsamis E, Sajda P, Hood DC. Enhancing the accuracy of glaucoma detection from OCT probability maps using convolutional neural networks. In: 2019 41st Annual International Conference of the IEEE Engineering in Medicine and Biology Society (EMBC). IEEE; 2019. p. 2036–40.
34. Park K, Kim J, Lee J. Visual field prediction using recurrent neural network. Sci Rep. 2019;9(1):1–12.
35. Sedai S, Antony B, Ishikawa H, Wollstein G, Schuman JS, Garnavi R. Forecasting retinal nerve fiber layer thickness from multimodal temporal data incorporating OCT volumes. Ophthalmol Glaucoma. 2020;3(1):14–24.
36. Chen Z, Wang Y, Wollstein G, de los Angeles Ramos-Cadena M, Schuman J, Ishikawa H. Macular GCIPL thickness map prediction via time-aware convolutional LSTM. In: 2020 IEEE 17th International Symposium on Biomedical Imaging (ISBI). IEEE; 2020. p. 1–5.
37. Uesaka T, Morino K, Sugiura H, Kiwaki T, Murata H, Asaoka R, Yamanishi K. Multi-view learning over retinal thickness and visual sensitivity on glaucomatous eyes. In: Proceedings of the 23rd ACM SIGKDD International Conference on Knowledge Discovery and Data Mining. 2017. p. 2041–50.
38. Sugiura H, Kiwaki T, Yousefi S, Murata H, Asaoka R, Yamanishi K. Estimating glaucomatous visual sensitivity from retinal thickness with pattern-based regularization and visualization. In: Proceedings of the 24th ACM SIGKDD International Conference on Knowledge Discovery & Data Mining. 2018. p. 783–92.
39. Christopher M, Bowd C, Belghith A, Goldbaum MH, Weinreb RN, Fazio MA, *et al*. Deep learning approaches predict glaucomatous visual field damage from OCT optic nerve head En face images and retinal nerve fiber layer thickness maps. Ophthalmology. 2020;127(3):346–56.

40. Maetschke S, Antony B, Ishikawa H, Wollstein G, Schuman J, Garnavi R. Inference of visual field test performance from OCT volumes using deep learning. arXiv preprint arXiv:1908.01428. 2019.
41. Christopher M, Proudfoot JA, Bowd C, Belghith A, Goldbaum MH, Rezapour J, *et al*. Deep learning models based on unsegmented OCT RNFL circle scans provide accurate detection of glaucoma and high resolution prediction of visual field damage. Invest Ophthalmol Vis Sci. 2020;61(7):1439.
42. Mendoza L, Christopher M, Belghith A, Bowd C, Rezapour J, Fazio MA, *et al*. Deep learning models predict age, sex and race from OCT optic nerve head circle scans. Invest Ophthalmol Vis Sci. 2020;61(7):2012.
43. Halupka KJ, Antony BJ, Lee MH, Lucy KA, Rai RS, Ishikawa H, *et al*. Retinal optical coherence tomography image enhancement via deep learning. Biomed Optics Express. 2018;9(12):6205–21.
44. Zeiler MD, Fergus R. Visualizing and understanding convolutional networks. In: European conference on computer vision. Cham: Springer; 2014. p. 818–33.
45. Simonyan K, Vedaldi A, Zisserman A. Deep inside convolutional networks: visualising image classification models and saliency maps. arXiv preprint arXiv:1312.6034. 2013.
46. Zhou B, Khosla A, Lapedriza A, Oliva A, Torralba A. Learning deep features for discriminative localization. In: Proceedings of the IEEE conference on computer vision and pattern recognition; 2016. p. 2921–9.
47. Bowd C, Chan K, Zangwill LM, *et al*. Comparing neural networks and linear discriminant functions for glaucoma detection using confocal scanning laser ophthalmoscopy of the optic disc. Invest Ophthalmol Vis Sci. 2002;43:3444–54.
48. Goldbaum MH, Sample PA, White H, Colt B, Raphaelian P, Fechtner RD, Weinreb RN. Interpretation of automated perimetry for glaucoma by neural network. Invest Ophthalmol Vis Sci. 1994;35(9):3362–73.
49. Chan K, Lee TW, Sample PA, Goldbaum MH, Weinreb RN, Sejnowski TJ. Comparison of machine learning and traditional classifiers in glaucoma diagnosis. IEEE Trans Biomed Eng. 2002;49(9):963–74.
50. Goldbaum MH, Sample PA, Chan K, Williams J, Lee TW, Blumenthal E, *et al*. Comparing machine learning classifiers for diagnosing glaucoma from standard automated perimetry. Invest Ophthalmol Vis Sci. 2002;43(1):162–9.
51. Aurenhammer F. Voronoi diagrams—a survey of a fundamental geometric data structure. ACM Computing Surveys (CSUR). 1991;23(3):345–405.
52. Townsend KA, Wollstein G, Danks D, *et al*. Heidelberg retina tomograph 3 machine learning classifiers for glaucoma detection. Br J Ophthalmol. 2008;92:814–8. https://doi.org/10.1136/bjo.2007.133074.
53. Zangwill LM, Chan K, Bowd C, *et al*. Heidelberg retina tomograph measurements of the optic disc and parapapillary retina for detecting glaucoma analyzed by machine learning classifiers. Invest Ophthalmol Vis Sci. 2004;45:3144–51. https://doi.org/10.1167/iovs.04-0202.
54. Uchida H, Brigatti L, Caprioli J. Detection of structural damage from glaucoma with confocal laser image analysis. Invest Ophthalmol Vis Sci. 1996;37:2393–401.
55. Adler W, Peters A, Lausen B. Comparison of classifiers applied to confocal scanning laser ophthalmoscopy data. Methods Inf Med. 2008;47:38–46. https://doi.org/10.3414/ME0348.
56. Bowd C, Zangwill LM, Medeiros FA, *et al*. Confocal scanning laser ophthalmoscopy classifiers and stereophotograph evaluation for prediction of visual field abnormalities in glaucoma-suspect eyes. Invest Ophthalmol Vis Sci. 2004;45:2255–62.
57. Weinreb RN, Zangwill L, Berry CC, *et al*. Detection of glaucoma with scanning laser polarimetry. Arch Ophthalmol. 1998;116:1583–9. https://doi.org/10.1001/archopht.116.12.1583.
58. Bowd C, Medeiros FA, Zhang Z, *et al*. Relevance vector machine and support vector machine classifier analysis of scanning laser polarimetry retinal nerve fiber layer measurements. Invest Ophthalmol Vis Sci. 2005;46:1322–9. https://doi.org/10.1167/iovs.04-1122.
59. Zhang Z, Yin FS, Liu J, Wong WK, Tan NM, Lee BH, *et al*. Origa-light: an online retinal fundus image database for glaucoma analysis and research. In: 2010 Annual International Conference of the IEEE Engineering in Medicine and Biology. IEEE; 2010. p. 3065–8.
60. Sng CC, Foo LL, Cheng CY, Allen JC, He M, Krishnaswamy G, Nongpiur ME, Friedman DS, Wong TY, Aung T. Determinants of anterior chamber depth: the Singapore Chinese Eye Study. Opthalmology. 2012;119(6):1143–50.
61. Chen X, Xu Y, Yan S, Wong DWK, Wong TY, Liu J. Automatic feature learning for glaucoma detection based on deep learning. In: International Conference on Medical Image Computing and Computer-Assisted Intervention. Cham: Springer; 2015. p. 669–77.

62. He K, Zhang X, Ren S, Sun J. Deep residual learning for image recognition. In: Proceedings of the IEEE conference on computer vision and pattern recognition. 2016. p. 770–8.
63. Ronneberger O, Fischer P, Brox T. U-net: Convolutional networks for biomedical image segmentation. In: International Conference on Medical image computing and computer-assisted intervention. Cham: Springer; 2015. p. 234–41.
64. Szegedy C, Vanhoucke V, Ioffe S, Shlens J, Wojna Z. Rethinking the inception architecture for computer vision. In: Proceedings of the IEEE conference on computer vision and pattern recognition; 2016. p. 2818–26.
65. Ren S, He K, Girshick R, Sun J. Faster r-cnn: towards real-time object detection with region proposal networks. In: Advances in neural information processing systems. 2015. p. 91–9.
66. Long J, Shelhamer E, Darrell T. Fully convolutional networks for semantic segmentation. In: Proceedings of the IEEE conference on computer vision and pattern recognition. 2015. p. 3431–40.
67. Bizios D, Heijl A, Hougaard JL, Bengtsson B. Machine learning classifiers for glaucoma diagnosis based on classification of retinal nerve fibre layer thickness parameters measured by Stratus OCT. Acta Ophthalmol. 2010;88(1):44–52.
68. Barella KA, Costa VP, Gonçalves Vidotti V, Silva FR, Dias M, Gomi ES. Glaucoma diagnostic accuracy of machine learning classifiers using retinal nerve fiber layer and optic nerve data from SD-OCT. J Ophthalmol. 2013.
69. Kotsiantis SB, Zaharakis I, Pintelas P. Supervised machine learning: a review of classification techniques. In: Maglogiannis I, *et al*., editors. Emerging Artificial Intelligence Applications in Computer Engineering. IOS Press; 2007. p. 3–24.
70. Brigatti L, Hoffman D, Caprioli J. Neural networks to identify glaucoma with structural and functional measurements. Am J Ophthalmol. 1996;121:511–21.
71. Bowd C, Hao J, Tavares IM, *et al*. Bayesian machine learning classifiers for combining structural and functional measurements to classify healthy and glaucomatous eyes. Invest Ophthalmol Vis Sci. 2008;49:945–53.
72. Leung CKS, Cheung CYL, Weinreb RN, Qiu K, Liu S, Li H, *et al*. Evaluation of retinal nerve fiber layer progression in glaucoma: a study on optical coherence tomography guided progression analysis. Invest Ophthalmol Vis Sci. 2010;51(1):217–22.
73. Na JH, Sung KR, Baek S, Lee JY, Kim S. Progression of retinal nerve fiber layer thinning in glaucoma assessed by cirrus optical coherence tomography-guided progression analysis. Curr Eye Res. 2013;38(3):386–95.
74. Caprioli J, Mock D, Bitrian E, Afifi AA, Yu F, Nouri-Mahdavi K, Coleman AL. A method to measure and predict rates of regional visual field decay in glaucoma. Invest Ophthalmol Vis Sci. 2011;52(7):4765–73.
75. Otarola F, Chen A, Morales E, Yu F, Afifi A, Caprioli J. Course of glaucomatous visual field loss across the entire perimetric range. JAMA ophthalmology. 2016;134(5):496–502.
76. Chen A, Nouri-Mahdavi K, Otarola FJ, Yu F, Afifi AA, Caprioli J. Models of glaucomatous visual field loss. Invest Ophthalmol Vis Sci. 2014;55(12):7881–7.
77. Warren JL, Mwanza JC, Tanna AP, Budenz DL. A statistical model to analyze clinician expert consensus on glaucoma progression using spatially correlated visual field data. Transl Vis Sci Technol. 2016;5(4):14.
78. Betz-Stablein BD, Morgan WH, House PH, Hazelton ML. Spatial modeling of visual field data for assessing glaucoma progression. Invest Ophthalmol Vis Sci. 2013;54(2):1544–53.
79. Anderson AJ. Comparison of three parametric models for glaucomatous visual field progression rate distributions. Transl Vis Sci Technol. 2015;4(4):2–2.
80. VanBuren J, Oleson JJ, Zamba GK, Wall M. Integrating independent spatio-temporal replications to assess population trends in disease spread. Stat Med. 2016;35(28):5210–21.
81. Wen JC, Lee CS, Keane PA, Xiao S, Rokem AS, Chen PP, *et al*. Forecasting future Humphrey visual fields using deep learning. PLoS One. 2019;14(4):e0214875.
82. Song Y, Ishikawa H, Wu M, Liu YY, Lucy KA, Lavinsky F, *et al*. Clinical prediction performance of glaucoma progression using a 2-dimensional continuous-time hidden markov model with structural and functional measurements. Ophthalmology. 2018;125(9):1354–61.
83. Hood DC, Kardon RH. A framework for comparing structural and functional measures of glaucomatous damage. Prog Retin Eye Res. 2007;26(6):688–710.
84. Zhu H, Crabb DP, Schlottmann PG, Lemij HG, Reus NJ, Healey PR, *et al*. Predicting visual function from the measurements of retinal nerve fiber layer structure. Invest Ophthalmol Vis Sci. 2010;51(11):5657–66.

85. Russell RA, Malik R, Chauhan BC, Crabb DP, Garway-Heath DF. Improved estimates of visual field progression using Bayesian linear regression to integrate structural information in patients with ocular hypertension. Invest Ophthalmol Vis Sci. 2012;53(6):2760–9.
86. Pollet-Villard F, Chiquet C, Romanet JP, Noel C, Aptel F. Structure-function relationships with spectral-domain optical coherence tomography retinal nerve fiber layer and optic nerve head measurements. Invest Ophthalmol Vis Sci. 2014;55(5):2953–62.

Source: Chen Z., Wollstein G., Schuman J.S., Ishikawa H. (2021) AI and Glaucoma. In: Grzybowski A. (eds) Artificial Intelligence in Ophthalmology. Springer, Cham. https://doi.org/10.1007/978-3-030-78601-4_9.

Efficacy and Safety of PreserFlo® MicroShunt After a Failed Trabeculectomy in Eyes with Primary Open-angle Glaucoma: A Retrospective Study

Luciano Quaranta, Eleonora Micheletti, Roberto Carassa, Carlo Bruttini, Riccardo Fausto, Andreas Katsanos, Ivano Riva

Abstract

Introduction: To evaluate the efficacy and safety of PreserFlo® MicroShunt in primary open angle glaucoma (POAG) eyes after a single failed trabeculectomy.
Methods: Retrospective review of POAG eyes with a failed trabeculectomy that underwent PreserFlo® MicroShunt implantation from March 2019 to November 2019, in two Italian glaucoma centers. Pre- and postoperative data were collected and compared.
Results: A total of 31 surgeries in 31 patients were reviewed. Mean preoperative IOP and mean preoperative number of medications were 24.12 ± 3.14 mmHg and 3.29 ± 0.64, respectively, and decreased to 12.56 ± 2.64 mmHg and 0.46 ± 0.77 at the 12-month postoperative follow-up visit ($p < 0.01$). The most frequent adverse events were transient hypotony (6 eyes, 19.3%) and choroidal effusion (3 eyes, 9.6%). In all cases spontaneous resolution was observed, with no intervention.
Conclusion: In POAG eyes with a single failed trabeculectomy, the PreserFlo® MicroShunt was safe and effective in reducing the IOP after a 12-month follow-up. The PreserFlo® MicroShunt may represent a viable choice as a second surgery.

Keywords: Glaucoma, MicroShunt; PreserFlo, Refractory glaucoma, Trabeculectomy

L. Quaranta (✉), E. Micheletti, C. Bruttini, R. Fausto
Department of Surgical and Clinical, Diagnostic and Pediatric Sciences, Section of Ophthalmology, University of Pavia-IRCCS Fondazione Policlinico San Matteo, Viale Camillo Golgi, 19, 27100 Pavia, Italy
e-mail: luciano.quaranta@unipv.it

R. Carassa
Centro Italiano Glaucoma, Milan, Italy

A. Katsanos
Department of Ophthalmology, University of Ioannina, Ioannina, Greece

I. Riva
IRCCS-Fondazione Bietti, Rome, Italy

Key Summary Points
Why carry out this study?
The optimal surgical management of eyes with primary open angle glaucoma after a failed trabeculectomy remains unknown. Available options include trabeculectomy revision or glaucoma drainage implant.
The PreserFlo® MicroShunt is a new surgical device implanted with a moderately invasive procedure.
The aim of the present study was to investigate the medium-term outcomes of PreserFlo® MicroShunt surgery in primary open-angle glaucoma eyes with a single failed trabeculectomy.
What was learned from the study?
The PreserFlo® MicroShunt is safe and effective in eyes with primary open angle glaucoma with a single failed trabeculectomy with a follow-up of 12 months. For this reason, it may be a viable choice as a second surgery in these eyes.

Introduction

Trabeculectomy, introduced by Cairns in 1968 [1], is the gold standard technique for the surgical management of open-angle glaucoma [2]. Although trabeculectomy has been demonstrated to be effective in reducing the intraocular pressure (IOP) [3-6], its efficacy tends to decrease over time, often requiring additional topical medical therapy.

When a trabeculectomy fails to achieve the target IOP despite a medical therapy, a second surgical intervention is needed. Available options in this case include revision of the previous trabeculectomy, a new trabeculectomy, or the use of a glaucoma drainage implant (GDI). Scarring processes, however, may have a detrimental effect on the revised trabeculectomy or the second trabeculectomy [7, 8]. In such cases, shunting the aqueous humor from the anterior chamber to the posterior subconjunctival space using a GDI may be advantageous, because the previously operated anterior conjunctiva is bypassed [9]. Unfortunately, this treatment strategy involves a considerably invasive procedure.

PreserFlo® MicroShunt (Santen, Osaka, Japan) is a new implantable device for IOP reduction in patients with open-angle glaucoma. The device is made of poly(styrene-*block*-isobutylene-*block*-styrene), a biocompatible, synthetic polymer also known as SIBS [10]. It is implanted *ab externo*, using a moderately invasive surgical approach. Mitomycin C (MMC) is also used during the implantation. The device redirects the aqueous humor posteriorly, and has been found to be effective at reducing IOP in initial non-comparative studies on glaucoma and ocular hypertensive eyes, with a low rate of complications, both in the short and in the long term [11-14]. As a result of the moderately invasive nature of the procedure compared to a trabeculectomy or a GDI, as well as the benefit of posterior aqueous humor redirection, the PreserFlo® MicroShunt may be a viable surgical option in eyes with a failed trabeculectomy.

The aim of the present study is to investigate the medium-term outcomes of PreserFlo® MicroShunt implantation in a group of primary open-angle glaucoma (POAG) eyes with a single failed trabeculectomy.

Methods

A retrospective chart review was conducted of PreserFlo® MicroShunt interventions after a single failed trabeculectomy, performed in two Italian glaucoma centers (IRCCS Policlinico San Matteo

Foundation and Hospital, Pavia, Italy, and Centro Italiano Glaucoma, Milan, Italy), between March 2019 and November 2019. As the design of the study was retrospective in nature, no ethics committee approval was required.

Inclusion criteria were a previous diagnosis of POAG, a single failed trabeculectomy performed at least 6 months previously, IOP ≥ 21 mmHg despite maximum tolerated medical therapy, and follow-up of at least 12 months after Preserflo® Microshunt implantation. POAG was defined as the presence of ophthalmoscopically abnormal optic disk (diffuse or focal thinning of the neuro-retinal rim), open angle at gonioscopy (Shaffer grade III or IV) along with the presence of abnormal visual field (VF) consistent with glaucoma. Maximum tolerated medical therapy was defined as at least three drugs, administered as either fixed- or unfixed combinations. Eyes that had undergone previous intraocular surgeries, with the exception of trabeculectomy and/or uncomplicated phacoemulsification, were excluded from the study.

For study enrollment, a reliable VF had to be performed within the previous 2 months (24–2 SITA Standard program, Humphrey Visual Field Analyzer, Carl Zeiss Meditec, Dublin, CA, USA). The severity of VF damage was classified according to the Glaucoma Staging System 2 (GSS2) [15-17]. The GSS2 classifies VF test into seven stages, by considering VF mean deviation (MD) and pattern standard deviation (PSD) on a Cartesian plot [16]. The perimetric stages are identified by curvilinear lines inside the plot, and range from stage 0 (within normal limits) to stage 5 (severely affected). In comparison to other VF staging systems (The Advanced Glaucoma Intervention Study scoring system [18] and the Hodapp-Anderson-Parrish system [19]), the GSS2 has been demonstrated to be preferable for its ease of use for clinicians and researchers alike [20]. Furthermore, it has been used in a number of population-based studies and clinical trials [21-23].

Collected data included patient demographics, pre- and postsurgical IOP, number of glaucoma medications, and Snellen visual acuity. Postoperative data were collected 1 day, 1 week, 1 month, 3 months, 6 months, and 12 months after PreserFlo® MicroShunt implantation. Surgical notes were reviewed for intraoperative complications. Postoperative complications were collected from the patient charts, and included transient hypotony (defined as an IOP < 6 mmHg without choroidal effusion and spontaneous resolution by 15 days), choroidal effusion, hyphema, shallow anterior chamber, stent exposure, and endophthalmitis.

Complete (i.e., without medications) and qualified (i.e., with or without medications) surgical success at 1 year was defined according to three IOP criteria: 1. IOP ≤ 17 mmHg and ≥ 6 mmHg, with ≥ 20% IOP reduction from baseline (first criterion); 2. IOP ≤ 14 mmHg and ≥ 6 mmHg, with ≥ 25% IOP reduction from baseline (second criterion); 3. IOP ≤ 12 mmHg and ≥ 6 mmHg, with ≥ 30% IOP reduction from baseline (third criterion).

The numbers of eyes requiring further surgical procedures in order to have the IOP controlled or the postoperative complications managed, following PreserFlo® implantation, were reported. Data from these eyes were analyzed exclusively until the last follow-up available before the new intervention. Moreover, these eyes were considered as failures in the calculation of the 1-year success rates.

Surgical Technique

Careful conjunctival assessment was performed before surgery, aiming at identifying the best surgical site, i.e., temporally or nasally with respect to the previous trabeculectomy. Conjunctival mobility, fibrosis, and the presence of active inflammation were factors taken into account to evaluate where the PreserFlo® could be implanted. A fornix-based sub-Tenon's flap was dissected over 90° to 120°, extending 8–10 mm posteriorly to the limbus. Three MMC-soaked sponges (0.3 mg/ml) were placed under the conjunctival flap for 3 min. After sponge removal, the tissue was meticulously rinsed with balanced salt solution. A reference point located 3 mm away from the surgical limbus was marked, and a shallow triangular pocket was incised through the sclera, using a 1-mm-width pre-calibrated knife. A trans-scleral tunnel was then dissected with a 25G needle, extending from the apex of the pocket to the anterior chamber. The PreserFlo® implant was then inserted and its fins were firmly wedged into the previously dissected scleral pocket. Filtration through the device was confirmed by observing aqueous humor percolation from its distal end. Finally, the conjunctiva and Tenon's capsule were stitched to the limbus using 10.0 nylon sutures. Betamethasone eyedrops were prescribed six times a day, and were gradually tapered over the following 4 months. Topical ofloxacin was administered four times a day for 15 days.

If needed, bleb needling was performed postoperatively at the slit-lamp using a 28G needle connected to a syringe, in order to penetrate the fibrous capsule around the distal end of the PreserFlo® MicroShunt, and thus restore aqueous humor flow through the device. Due attention was paid to avoid inadvertent perforation of the overlying conjunctiva and piercing subconjunctival blood vessels. In case of extensive scarring, a 0.1 ml solution containing an antimetabolite drug (50 mg/ml 5-fluorouracil (5FU) or 0.2 mg/ml MMC) was injected underneath the conjunctiva, at the end of the procedure. Following a negative or minimally positive Seidel test, the eye was patched with tobramycin antibiotic ointment until the next morning.

Statistical Analysis

Continuous variables were described as mean and standard deviation (SD). Categorical variables were reported as frequency and percentage. Continuous variables were tested for normality using the Shapiro–Wilk test. A non-parametric Wilcoxon signed rank test was used to compare baseline vs. postoperative data, as non-normal distribution of continuous variables was found. Taking into account the number of comparisons, a Bonferroni correction was applied.

Relationships between preoperative IOP, number of medications, time from previous trabeculectomy, and 1-year follow-up IOP (outcome variable) were evaluated using univariate linear regression. Normal distribution of residuals was tested using the Shapiro-Wilk test, the Kolmogorov-Smirnov test, and the Anderson-Darling test, in addition to the visual inspection of the residual plot. Homogeneity of error variance was confirmed by examining the spread-location plot of residuals. One outlier was identified in the outcome variable (standardized residual > 3), and thus excluded from the analysis. All analyses were performed using R-project for Statistical Computing (R Core Team (2013), Vienna, Austria. http://www.R-project.org/).

Results

Thirty-one pseudophakic eyes (31 patients) with a single failed trabeculectomy received PreserFlo® MicroShunt between March 2019 and November 2019 (Table 1), and were followed up for a mean of 13.35 ± 1.08 months. All patients were Caucasian, with a mean age of 67.98 ± 11.35 years. Trabeculectomy with MMC had been performed on average 32.77 ± 14.57 months before (range 7.7–66.0). According to the GSS2, VF before Preserflo® Microshunt implantation was classified as stage 2 in 3 eyes (9.68%), stage 3 in 23 eyes (74.19%), and stage 4 in 5 eyes (16.13%).

The PreserFlo® MicroShunt was positioned temporally with respect to the previous trabeculectomy, in 29 eyes (93.5%), and nasally in 2 eyes (6.4%). The mean preoperative and postoperative IOP and number of IOP-lowering medications are reported in Fig. 1. No relationship was found between the IOP at the 1-year follow-up visit and preoperative IOP ($p = 0.18$), number of IOP-lowering medications preoperatively ($p = 0.56$), and time from previous trabeculectomy

Table 1: Patient characteristics.

No. of eyes (patients)	31 (31)
Age in years, mean (SD)	67.98 (11.35)
Race	
White, *n* (%)	31 (100%)
Sex	
Men, *n* (%)	14 (45.1)
Women, *n* (%)	17 (54.8)
Eye	
Right, *n* (%)	17 (54.8)
Left, *n* (%)	14 (45.1)
Time from trabeculectomy (months)	
Mean (SD)	32.77 (14.57)
Minimum–maximum	7.7–66.0
IOP (mmHg), mean (SD)	24.8 (3.86)
Visual field MD (dB), mean (SD)	−6.17 (1.88)
Visual filed PSD (dB), mean (SD)	8.85 (2.12)
Stage of the disease (GSS2), *n* (%)	
Stage 2	3 (9.68)
Stage 3	23 (74.19)
Stage 4	5 (16.13)
Number of glaucoma medications (SD)	3.29 (0.64)
BCVA, decimal notation (SD)	0.57 (0.19)
Site of implantation	
Temporal *n* (%)	29 (93.5%)
Nasal *n* (%)	2 (6.4%)

SD standard deviation, *IOP* intraocular pressure, *MD* mean deviation, *PSD* pattern standard deviation, *GSS2* Glaucoma Staging System 2, *BCVA* best corrected visual acuity

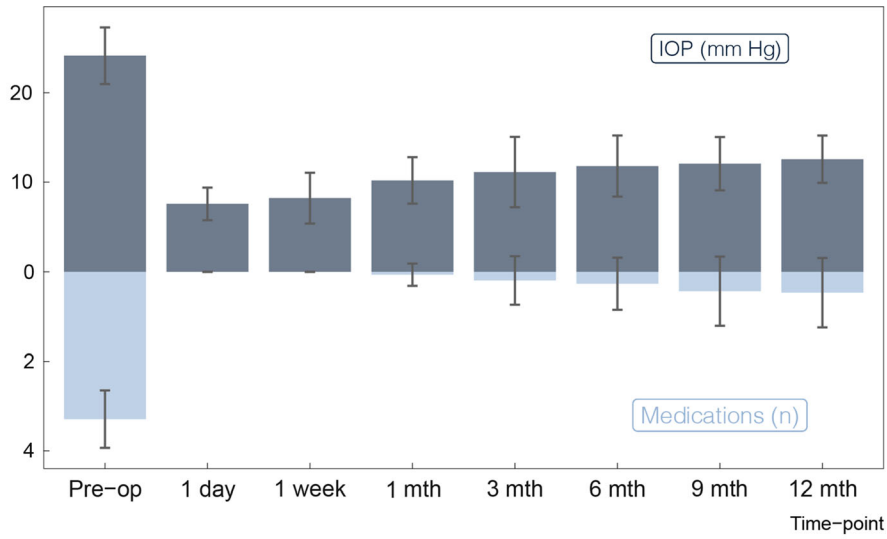

Mean IOP (mm Hg) (SD)	24.12 (3.14)	7.58 (1.8)	8.22 (2.82)	10.19 (2.6)	11.12 (3.93)	11.8 (3.41)	12.0 (2.98)	12.56 (2.64)
Comparison to pre-op IOP		p<0.01	p<0.01	p<0.01	p<0.01	p<0.01	p<0.01	p<0.01
Mean n. of meds (SD)	3.29 (0.64)	0 (0)	0 (0)	0.06 (0.24)	0.19 (0.54)	0.26 (0.58)	0.43 (0.77)	0.46 (0.77)
Comparison to pre-op meds		p<0.01	p<0.01	p<0.01	p<0.01	p<0.01	p<0.01	p<0.01

Fig. 1: Mean IOP and mean number of IOP-lowering medications throughout the study. Wilcoxon signed rank test was used to compare baseline vs. postoperative data. IOP intraocular pressure, meds medications, SD standard deviation, mth month.

Fig. 2: Scatter plot of preoperative IOP versus IOP at 1-year follow-up, according to preoperative number of medications. Censored for reoperations ($n = 1$). IOP Intraocular pressure, meds medications.

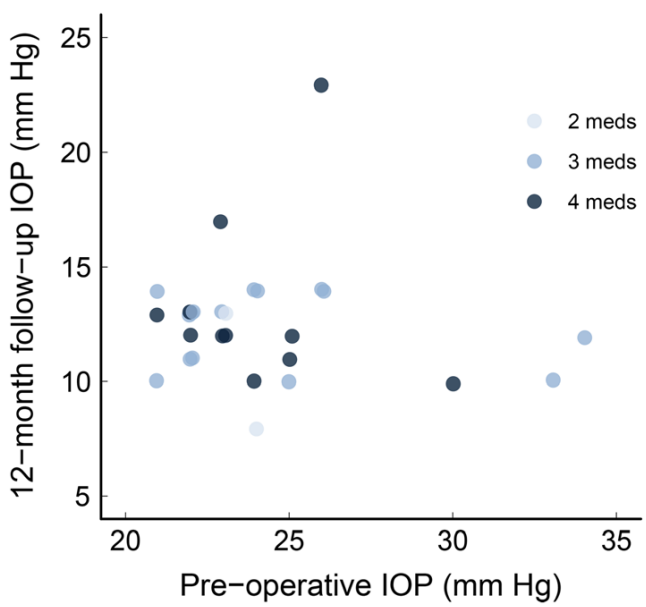

($p = 0.24$). Figure 2 shows a scatter plot of preoperative IOP versus 1-year follow-up IOP, taking into account the number of preoperative IOP-lowering medications.

Considering the success criteria at 1 year, 67.74%, 67.74%, and 45.16% of the eyes achieved complete success for the first (6–17 mmHg), second (6–14 mmHg), and third (6–12 mmHg) criteria, respectively. Qualified success was achieved by 93.54%, 90.32%, and 48.38% of the eyes, when the respective success criteria were taken into account.

Of the 31 eyes undergoing surgery, 6 eyes (19.3%) returned to baseline visual acuity by 1 week, 6 eyes (19.3%) by 1 month, and 19 eyes (61.2%) by 3 months. None of the operated eyes experienced central visual acuity loss. One eye underwent one surgical revision of the PreserFlo® MicroShunt implant 4 months after the initial surgery because of uncontrolled IOP despite maximum tolerated medical therapy and bleb needling with antimetabolite.

The most frequent adverse event was transient hypotony (6 eyes, 19.3%). Choroidal effusion was documented in 3 eyes (9.6%); among them, one eye (3.2%) had shallow anterior chamber. Hyphema was reported in 1 eye (3.2%). All these complications resolved spontaneously. A total of 9 bleb needlings were performed in 6 eyes (19.3%). Three eyes (9.6%) received a single needling procedure, and 3 eyes (9.6%) received 2 needling procedures. Needling was augmented with 5FU in 2 eyes and with MMC in 1 eye. There was no case of stent exposure, hypotony maculopathy, persistent choroidal effusions, or endophthalmitis. No intraoperative complications were recorded.

Discussion

The optimal surgical management of eyes with a failed trabeculectomy remains poorly defined. Trabeculectomy revision has been shown to be not particularly effective, likely because of the exaggerated healing response [8]. Conceptually, a GDI may have more chance of success, as it directs the aqueous humor posteriorly, away from perilimbal areas with extensive fibrosis.

The tube vs. trabeculectomy (TVT) study recruited patients with primary or secondary glaucoma and uncontrolled IOP (between 18 and 40 mmHg) who had previously undergone trabeculectomy or cataract extraction (mostly intra- and extracapsular techniques) [24]. A total of 212 eyes of 212 patients were enrolled in 17 centers, and randomized to Baerveldt GDI (350 mm^2, 107 eyes) or trabeculectomy plus MMC (0.4 mg/mL for 4 min, 105 eyes). Both interventions were similarly effective at reducing the IOP from 3 months postoperatively to the end of the follow-up, with a 5-year IOP of 14.4 ± 6.9 mmHg and 12.6 ± 5.9 mmHg in the tube and in the trabeculectomy group, respectively ($p = 0.12$) [25]. The surgical safety profile was similar for both groups, with no difference in terms of number of serious complications over the entire follow-up [25]. The results of the TVT study supported the notion that GDIs could be used earlier in the natural history of glaucoma, and not only in eyes that have already undergone glaucoma surgical procedures [26]. However, tube surgery remains particularly invasive, and may be associated with serious complications, such as hypotony, loss of central visual acuity, diplopia, corneal endothelial damage, and tube erosion [9, 25, 27]. In addition, a report by the American Academy of Ophthalmology has suggested that when a very low IOP is desired, a GDI may be a poor choice, because the IOP generally tends to settle at higher levels than after a trabeculectomy [28].

Nassiri *et al.* compared the efficacy and safety of a second trabeculectomy plus MMC vs. an Ahmed GDI in patients with a previous failed trabeculectomy [29]. At the 3-year follow-up visit, the IOP was reduced by 42.21% and 43.12% from baseline in the trabeculectomy and the GDI group, respectively ($p = 0.42$). The mean number of IOP-lowering medications at 3 years was 2.11 ± 1.73 and 2.20 ± 1.64, respectively, in the trabeculectomy and in the GDI group, with no between-group difference ($p = 0.82$). Although more eyes in the trabeculectomy group experienced postoperative complications (46.15% of the eyes in the trabeculectomy group vs. 30% of the eyes in the GDI group, $p = 0.03$), there was no significant difference in terms of number of complications, with the exception of wound leakage, occurring more frequently in eyes in the trabeculectomy group.

In our study, PreserFlo® MicroShunt was demonstrated to be effective at reducing IOP in eyes with POAG and a single failed trabeculectomy. Indeed, the IOP decreased significantly by 47.93% from baseline to the 1-year follow-up, and the mean number of medications also decreased significantly from 3.29 to 0.46. Relatively mild complications were encountered only at the postoperative period. The most frequent of these were transient hypotony and choroidal effusion. The IOP reduction and the decrease in the number of medications documented in our study were similar or better than those reported in both the TVT [25] and the Nassiri *et al.* [29] studies. Importantly, the safety profile of the procedure in our study was apparently better than the ones described in the TVT [25] and in the Nassiri *et al.* [29] trials. In the TVT study, serious complications (defined as ones requiring reoperation and/or causing loss of two or more Snellen lines) occurred in 22% and 20% of the enrolled eyes during the 5-year follow-up in the tube and in the trabeculectomy group, respectively ($p = 0.79$) [25]. Although the rate of serious complications in the study by Nassiri *et al.* was not reported, 7 eyes (10.7%) in the trabeculectomy group and 3 eyes (5%) in the Ahmed GDI group had more than one complication [29]. Moreover, at the end of the 3rd year of follow-up, 3 eyes (4.6%) in the trabeculectomy group and 2 eyes (3%) in the Ahmed GDI group had experienced loss of light perception. The comparison of our results with those of these studies, however, should be cautious, mainly because of the small sample size of our study and the relatively short-term follow-up.

In a recent study by Durr *et al.*, the efficacy and safety of PreserFlo® MicroShunt were evaluated in 85 eyes with primary or secondary glaucoma that had already undergone at least one surgical procedure (i.e., cyclophotocoagulation, trabecular bypass, trabeculectomy, GDI implant) [30]. At the 1-year follow-up visit, eyes implanted with PreserFlo® MicroShunt had a mean IOP of 13.5 mmHg with a mean of 0.9 medications (interquartile range 0–2). Sixty-one percent and 79.7% of the eyes achieved complete (without medications) and qualified (with medications) success, with failure being defined as IOP < 6 mmHg with vision loss, IOP > 17 mmHg, or IOP reduction < 20% from baseline. Needling plus MMC was performed in 11.8% of the eyes, and surgical bleb revision was undertaken in 4.7% of eyes ($n = 4$). The most frequent complications were choroidal effusion (11 eyes, 12.9%), shallow anterior chamber (8 eyes, 9.4%), hyphema (7 eyes, 8.2%), and hypotony maculopathy (3 eyes, 3.5%). A comparison of these results with ours is difficult, as we only enrolled patients with POAG and a single previous trabeculectomy. The IOP reduction after 1 year of follow-up in our study was similar and even better than the IOP reduction

observed by Durr *et al.* [30]. Additionally, early hypotony was the most frequent complication in both studies. This adverse event may be relatively frequent with this type of surgery because of the lack of a valve mechanism embedded into the device.

Karimi *et al.* recently published a retrospective review of 17 eyes with primary or secondary glaucoma that underwent Xen® gel stent implantation after a failed trabeculectomy [31]. In this study, the IOP decreased from 21.5 ± 2.4 preoperatively to 13.6 ± 3.4 mmHg ($p < 0.05$) at 12 months (36.8% reduction from baseline), while the mean number of IOP-lowering medications decreased from 2.8 ± 0.6 to 1.0 ± 1.3 ($p < 0.05$). The most frequent complications were transient hypotony (23.5%), postoperative IOP spike (11.8%), and surgical failure (11.8%), requiring new interventions to control IOP. One eye (6%) lost one line, and 1 eye (6%) lost three lines of Snellen visual acuity by month 6. A mean of 2.4 bleb needlings/antimetabolite injections were required per eye to control the IOP. Because the Xen® gel stent and the PreserFlo® MicroShunt are different devices, with dissimilar design, and each requires a different surgical technique, the results of our study are not comparable to the results by Karimi *et al.* [31].

Limitations of the current study include its retrospective design, the small sample size, and the medium-term follow-up. Moreover, our results may not be valid in eyes affected by other types of glaucoma than POAG.

Conclusion

The current study suggests that PreserFlo® MicroShunt in eyes with POAG and a single failed trabeculectomy is effective in reducing IOP after a follow-up of 12 months, with a favorable safety profile. As PreserFlo® MicroShunt surgery is less invasive in comparison to GDI surgery or trabeculectomy, it may represent a viable choice as a second surgery in these eyes. Further studies, with a greater sample size and a longer follow-up are warranted to confirm these first results. In addition, data about the comparative efficacy and safety of PreserFlo® versus other surgical options (e.g., second trabeculectomy, Xen or GDI implantation) in eyes with a failed trabeculectomy are needed.

Acknowledgements

Funding: Open access funding provided by Università degli Studi di Pavia within the CRUI-CARE Agreement. The contribution of the Fondazione Bietti in this study was supported by Ministry of Health and Fondazione Roma, Italy.

Authorship: All named authors meet the International Committee of Medical Journal Editors (ICMJE) criteria for authorship for this article, take responsibility for the integrity of the work as a whole, and have given their approval for this version to be published.

Authors' Contributions: Conceptualization: Luciano Quaranta, Ivano Riva; Methodology: Luciano Quaranta, Ivano Riva, Roberto Carassa; Formal analysis and investigation: Eleonora Micheletti, Luciano Quaranta, Ivano Riva; Writing—original draft preparation: Carlo Bruttini, Riccardo Fausto, Eleonora Micheletti, Ivano Riva; Writing—review and editing: Andreas Katsanos, Luciano Quaranta, Ivano Riva; Supervision: Luciano Quaranta, Ivano Riva.

Disclosures: Luciano Quaranta: Fee/Honoraria from Allergan, Bausch&Lomb, Novartis, Thea, Santen, Visufarma; Consultancy for Fidia-Sooft, Visufarma; Travel/Research grant from Allergan, Bausch&Lomb, Omikron, Novartis, Santen, SIFI. Roberto Carassa: Fee/Honoraria from Allergan, Fidia-Sooft, Omikron, Santen; Andreas Katsanos: Honoraria and congress expenses from Santen, Vianex, Zwitter; Research grant from Laboratoires Théa. Ivano Riva: Honoraria and congress expenses from Allergan, Santen, Visufarma, SIFI. Eleonora Micheletti, Carlo Bruttini and Riccardo Fausto declare that they have no conflict of interest.

Compliance with Ethics Guidelines: All procedures performed in this study were in accordance with the ethical standards of the institutional and/or national research committee and with the 1964 Helsinki declaration and its later amendments or comparable ethical standards. As the design of the study was retrospective in nature, no ethics committee approval was required.

Data Availability: All authors had full access to all of the data in this study and take complete responsibility for the integrity of the data and accuracy of the data analysis. The datasets generated and/or analyzed during the current study are available from the corresponding author on reasonable request.

References

1. Cairns JE. Trabeculectomy. Preliminary report of a new method. Am J Ophthalmol. 1968;66(4):673–9.
2. Rulli E, Biagioli E, Riva I, *et al*. Efficacy and safety of trabeculectomy vs nonpenetrating surgical procedures: a systematic review and meta-analysis. JAMA Ophthalmol. 2013;131(12):1573–82.
3. Edmunds B, Thompson JR, Salmon JF, Wormald RP. The National survey of trabeculectomy. II. Variations in operative technique and outcome. Eye (Lond). 2001;15(Pt 4):441–8.
4. Scott IU, Greenfield DS, Schiffman J, *et al*. Outcomes of primary trabeculectomy with the use of adjunctive mitomycin. Arch Ophthalmol. 1998;116(3):286–91.
5. Wilensky JT, Chen TC. Long-term results of trabeculectomy in eyes that were initially successful. Trans Am Ophthalmol Soc. 1996;94:147–59 (discussion 60–4).
6. Molteno AC, Bosma NJ, Kittelson JM. Otago glaucoma surgery outcome study: long-term results of trabeculectomy–1976 to 1995. Ophthalmology. 1999;106(9):1742–50.
7. Law SK, Shih K, Tran DH, Coleman AL, Caprioli J. Long-term outcomes of repeat vs initial trabeculectomy in open-angle glaucoma. Am J Ophthalmol. 2009;148(5):685-95 e1.
8. Hirunpatravong P, Reza A, Romero P, *et al*. Same-site trabeculectomy revision for failed trabeculectomy: outcomes and risk factors for failure. Am J Ophthalmol. 2016;170:110–8.
9. Riva I, Roberti G, Oddone F, Konstas AG, Quaranta L. Ahmed glaucoma valve implant: surgical technique and complications. Clin Ophthalmol. 2017;11:357–67.
10. Do AT, Parikh H, Panarelli JF. Subconjunctival microinvasive glaucoma surgeries: an update on the Xen gel stent and the PreserFlo MicroShunt. Curr Opin Ophthalmol. 2020;31(2):132–8.
11. Riss I, Batlle J, Pinchuk L, Kato YP, Weber BA, Parel JM. One-year results on the safety and efficacy of the InnFocus MicroShunt depending on placement and concentration of mitomycin C. J Fr Ophtalmol. 2015;38(9):855–60.
12. Batlle JF, Fantes F, Riss I, *et al*. Three-year follow-up of a novel aqueous humor microshunt. J Glaucoma. 2016;25(2):e58-65.
13. Scheres LMJ, Kujovic-Aleksov S, Ramdas WD, *et al*. XEN((R)) Gel Stent compared to PRESERFLO MicroShunt implantation for primary open-angle glaucoma: two-year results. Acta Ophthalmol. 2021;99(3):e433–e440.
14. Batlle JF, Corona A, Albuquerque R. Long-term results of the PRESERFLO(R) MicroShunt in patients with primary open-angle glaucoma from a single-center non-randomized study. J Glaucoma. 2021;30(3):281–6.
15. Brusini P. Clinical use of a new method for visual field damage classification in glaucoma. Eur J Ophthalmol. 1996;6(4):402–7.
16. Brusini P, Filacorda S. Enhanced glaucoma staging system (GSS 2) for classifying functional damage in glaucoma. J Glaucoma. 2006;15(1):40–6.
17. Brusini P, Johnson CA. Staging functional damage in glaucoma: review of different classification methods. Surv Ophthalmol. 2007;52(2):156–79.
18. Advanced Glaucoma Intervention Study. 2. Visual field test scoring and reliability. Ophthalmology. 1994;101(8):1445–55.
19. Hodapp E, Parrish RK, Anderson D. Clinical decisions in glaucoma. 1st ed. St Louis: Mosby; 1993.
20. Ng M, Sample PA, Pascual JP, *et al*. Comparison of visual field severity classification systems for glaucoma. J Glaucoma. 2012;21(8):551–61.

21. Rulli E, Quaranta L, Riva I, *et al*. Visual field loss and vision-related quality of life in the Italian primary open angle glaucoma study. Sci Rep. 2018;8(1):619.
22. Le PV, Zhang X, Francis BA, *et al*. Advanced imaging for glaucoma study: design, baseline characteristics, and inter-site comparison. Am J Ophthalmol. 2015;159(2):393-403 e2.
23. Roh KH, Jeoung JW, Park KH, Yoo BW, Kim DM. Long-term reproducibility of cirrus HD optical coherence tomography deviation map in clinically stable glaucomatous eyes. Ophthalmology. 2013;120(5):969–77.
24. Gedde SJ, Chen PP, Heuer DK, *et al*. The primary tube versus trabeculectomy study: methodology of a multicenter randomized clinical trial comparing tube shunt surgery and trabeculectomy with mitomycin C. Ophthalmology. 2018;125(5):774–81.
25. Gedde SJ, Singh K, Schiffman JC, Feuer WJ, Tube Versus Trabeculectomy Study Group. The Tube Versus Trabeculectomy Study: interpretation of results and application to clinical practice. Curr Opin Ophthalmol. 2012;23(2):118–26.
26. Gedde SJ, Kornmann HL. Glaucoma surgery in pseudophakic eyes: tube shunt first. Surv Ophthalmol. 2017;62(1):108–12.
27. Caprioli J. The tube versus trabeculectomy study: why its findings may not change clinical practice? Am J Ophthalmol. 2011;151(5):742-4 e1.
28. Minckler DS, Francis BA, Hodapp EA, *et al*. Aqueous shunts in glaucoma: a report by the American Academy of Ophthalmology. Ophthalmology. 2008;115(6):1089–98.
29. Nassiri N, Syeda S, Tokko H, *et al*. Three-year outcomes of trabeculectomy and Ahmed valve implant in patients with prior failed filtering surgeries. Int Ophthalmol. 2020;40(12):3377–91.
30. Durr GM, Schlenker MB, Samet S, Ahmed IIK. One-year outcomes of stand-alone ab externo SIBS microshunt implantation in refractory glaucoma. Br J Ophthalmol. 2020. https://doi.org/10.1136/bjophthalmol-2020-317299.
31. Karimi A, Hopes M, Martin KR, Lindfield D. Efficacy and safety of the ab-interno Xen Gel stent after failed trabeculectomy. J Glaucoma. 2018;27(10):864–8.

Source: Quaranta, L., Micheletti, E., Carassa, R. *et al*. Efficacy and Safety of PreserFlo® MicroShunt After a Failed Trabeculectomy in Eyes with Primary Open-Angle Glaucoma: A Retrospective Study. *Adv Ther* **38**, 4403–4412 (2021). https://doi.org/10.1007/s12325-021-01811-w.

Congenital Glaucoma and Anterior Segment Dysgenesis

Chirakshi Dhull, Sudarshan Kumar Khokhar

Childhood cataract may occur in association with ocular comorbidities involving cornea, angle structures, and/or iris. These abnormalities may include congenital glaucoma and anterior segment dysgenesis. These associated abnormalities may alter presentation and management of these conditions. In this chapter, we will discuss these two entities in separate section. They have been clubbed together since anterior segment dysgenesis is associated with glaucoma in significant number of cases and few cases of presumed primary congenital glaucoma may actually be secondary to anterior segment dysgenesis.

Childhood Glaucoma

- Introduction
- Clinical presentation
- Investigations
- Surgical outcomes

Introduction

Primary congenital glaucoma (PCG) is an anomaly affecting anterior chamber angle which leads to obstruction of aqueous outflow, increased intraocular pressure (IOP) and optic nerve damage [1]. Buphthalmos is an alternate term used to describe congenital glaucoma. Buphthalmos means "bull's eye." It is used to describe visible enlargement of the eyeball and clouding of cornea at birth or early childhood due to uncontrolled glaucoma [2]. High intraocular pressure (IOP) causes increase in axial length and corneal dimensions of the eye, leading to axial myopia, stretched limbus, corneal thinning and visibly enlarged eyeballs. The common causes of buphthalmos

Supplementary Information The online version of this chapter (https://doi.org/10.1007/978-981-16-0212-2_15) contains supplementary material, which is available to authorized users.

C. Dhull (✉)
Eye Q Hospital, Rohtak, Haryana, India

S. K. Khokhar
Professor Ophthalmology, Dr. RP Centre for Ophthalmic Sciences, All India Institute of Medical Sciences, New Delhi, India

include primary congenital glaucoma (PCG), Sturge-Weber syndrome, neurofibromatosis, and aniridia [2].

Incidence of PCG is one in every 10,000–15,000 live births which accounts for 0.01–0.04% of total blindness [3]. It is bilateral in up to 80% of cases and two-third of cases are males. Most cases are sporadic (90%) [4]. However, in the remaining 10%, there appears to be a strong familial component.

Clinical Presentation

PCG patients may present with corneal haze, enlarged eye size, or abnormal eye movements. Vision loss in these eyes may occur secondary to uncorrected refractive error, corneal opacity, optic nerve damage, amblyopia, and cataracts. Cataract may be congenital/developmental or as a sequalae to glaucoma filtration surgery. Examination findings may be variable.

- Progressive myopia and high astigmatism may be seen.
- Cornea may be hazy and presence of Haab striae is a common finding (Fig. 1).
- Cataract may be anterior or posterior subcapsular cataract, total or less commonly cortical or zonular cataract (Fig. 2). Cataract may be primary or more commonly secondary to trabeculectomy in 6–58% cases [5-7]. Zonular weakness may be present.
- Bleb in post trabeculectomy eyes with buphthalmos may be thin cystic and rarely associated with other complications (Fig. 3).
- Fundus examination may reveal advanced cupping. The cupping may be reversible in small children. Features associated with pathological myopia may be seen.

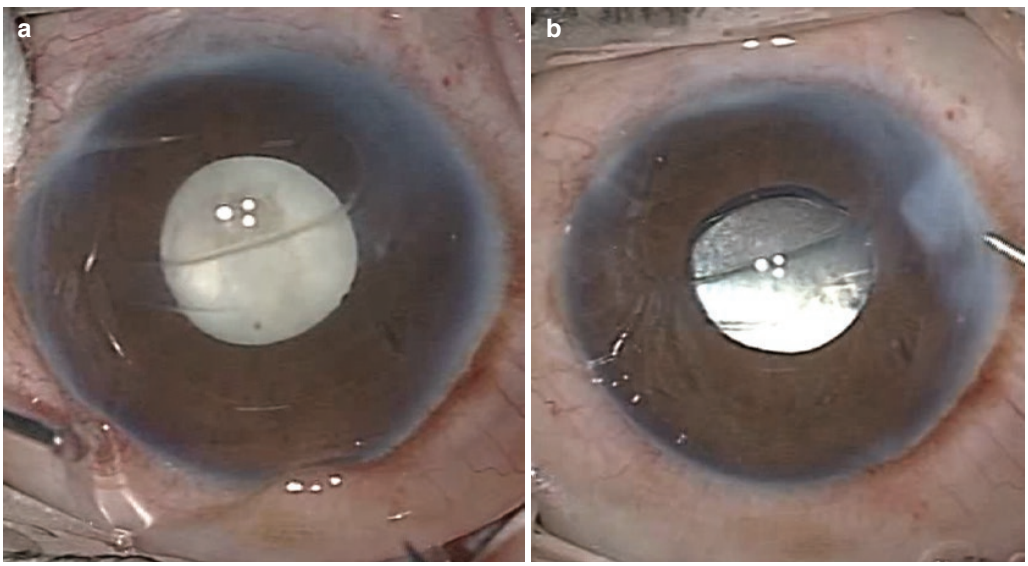

Fig. 1: Congenital glaucoma with Haab striae and total cataract. (**a**) Preoperative picture where large superior and multiple peripheral Haab striae. (**b**) Postoperative picture with IOL in situ and more pronounced Haab striae.

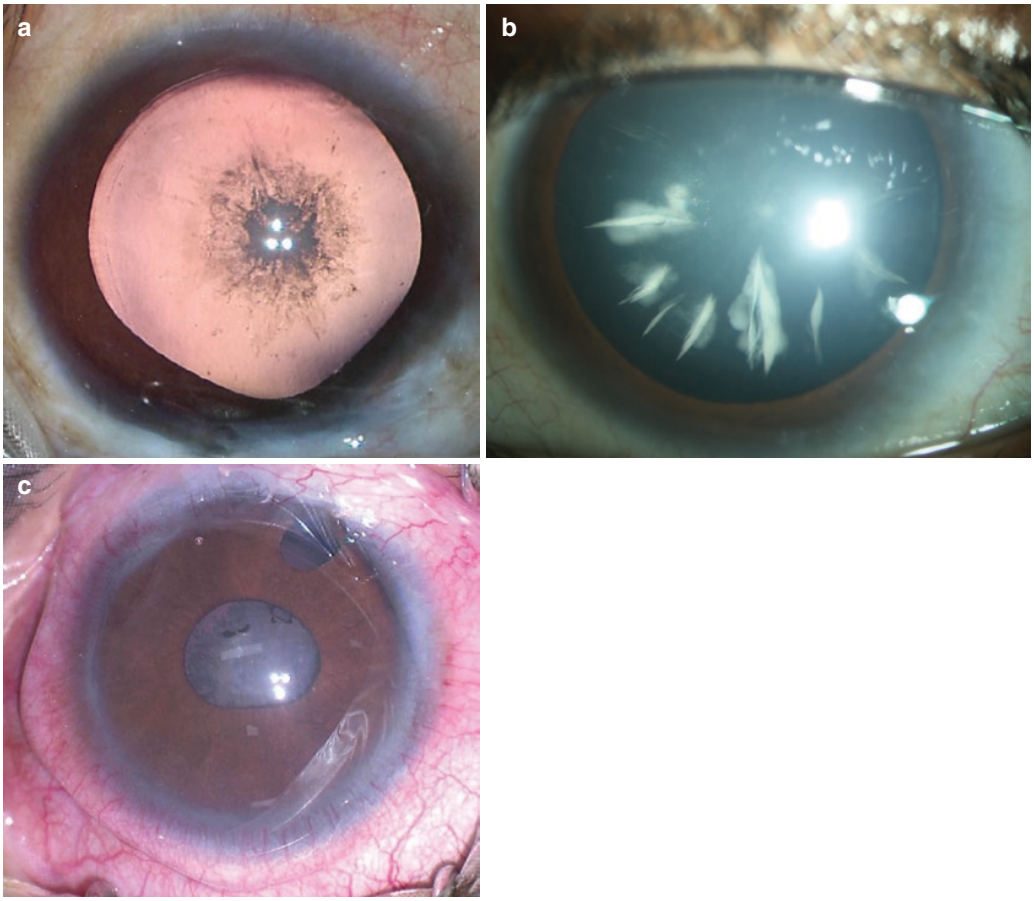

Fig. 2: Morphology in cataract with childhood glaucoma post trabeculectomy. (**a**) Posterior subcapsular cataract. (**b**) Cortical cataract. (**c**) Diffuse cataract with large superonasal peripheral iridotomy.

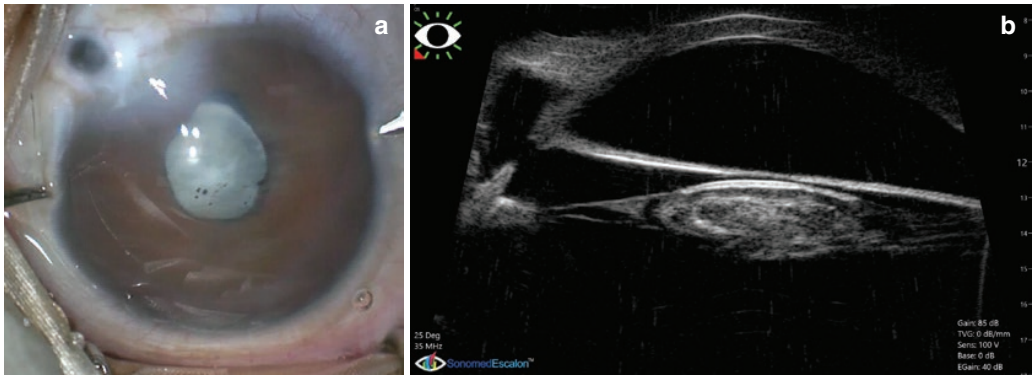

Fig. 3: Post trabeculectomy thin cystic bleb with iris prolapse from the ostium and total cataract. (**a**) Clinical picture. (**b**) Ultrasound biomicroscopy of the same showing patent ostium and elevated bleb.

Investigations

In addition to usual investigations, Ultrasound biomicroscopy (UBM) can be used for measurement of angle to angle and bag diameter and aid in planning of surgery (Fig. 4). UBM also helps to assess anterior segment structures, anterior chamber depth (ACD), angle anomalies, abnormal iris insertion, helps assess sulcus-to-sulcus measurement and identifies lax zonules and posterior capsular defect preoperatively [8].

Management of Cataract in Buphthalmic Eyes

Apart from the routine challenges encountered, there are additional surgical difficulties faced by surgeon while operating cataract in buphthalmic eyes. These include the following:

- **Corneal haze** may cause difficulty in visualization during surgery (Fig. 5). IOP should be controlled before surgery. We recommend use of dye for staining of anterior capsule in such cases. Posterior capsule may also require staining if visibility is low.
- **Very deep anterior chamber (AC)** may result in difficult instrumentation. Intraoperatively, anterior chamber depth may show frequent fluctuations due to low scleral rigidity. We use microincision forceps with longer arm compared to utrata's forceps for capsulorhexis. Use of bimanual irrigation and aspiration provides better control to the situation.
- **Zonular weakness:** Phacodonesis, lax lens zonules, liquefied vitreous and, thus, a weak posterior capsular support can lead to inadvertent complications. There is increased risk of vitreous loss in these patients.

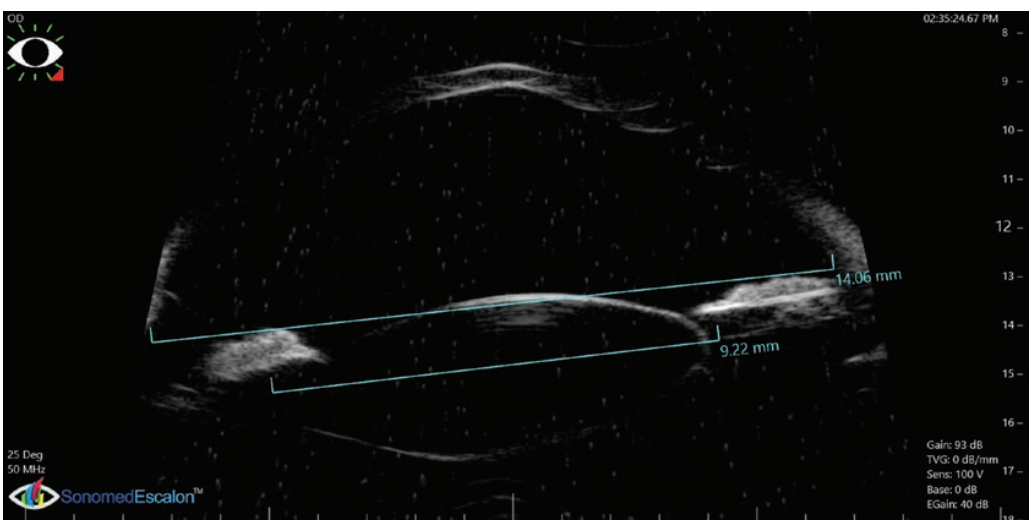

Fig. 4: Ultrasound biomicroscopy showing dimensions of buphthalmic eye. Complete white to white examination is not possible in single view. (**a**) Angle to angle distance, (**b**) bag diameter.

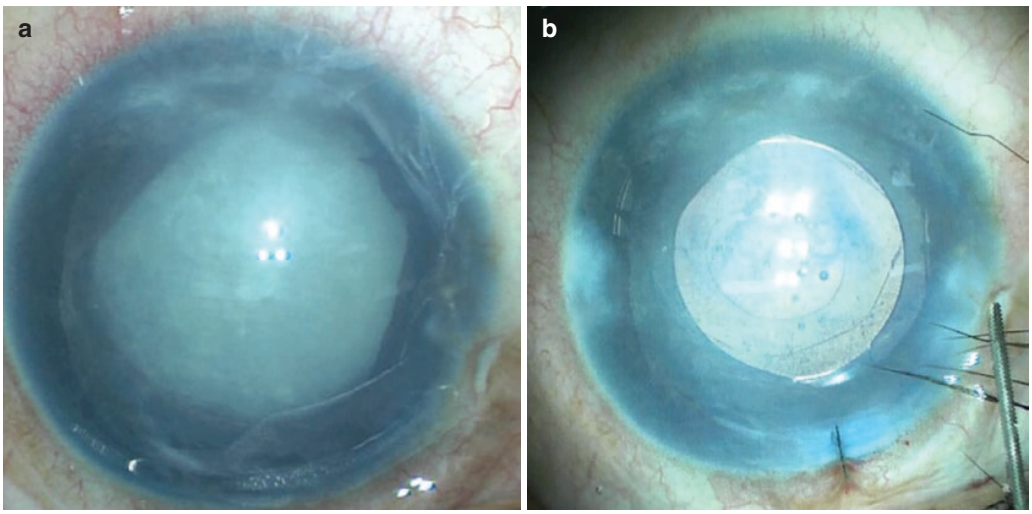

Fig. 5: Six-year-old child with congenital glaucoma with corneal haze with atrophic iris. (**a**) Preoperative picture with total cataract. (**b**) Postoperative picture with circular anterior and posterior capsulorhexis and IOL in bag.

- **Wound apposition:** Bupththalmic eyes have thin sclera and cornea. Hydration alone does not provide sufficient wound closure in most cases. We recommend suturing of main wound as well as side port to prevent postoperative shallow AC.
- **IOL power calculation** remains difficult. Post-trabeculectomy buphthalmic eyes have a shift towards with-the rule astigmatism [9, 10]. As most of these eyes are high myopic, IOL power calculation should be done using appropriate IOL formulae e.g., SRK-T for axial lengths >24.5 mm. Many a times, no single IOL power formulae might be able to predict the correct emmetropic power of implant for buphthalmic eyes. Parents should be counseled preoperatively, regarding use of spectacles for distance and near vision.
- Large eye size and bag dimensions that may lead to postoperative intraocular lens (IOL) decentration [11, 12]. In the bag IOL placement with posterior capsulorhexis has been reported to be associated with decentration. The technique of IOL implantation in the sulcus with optic capture with anterior or both anterior and posterior capsule (i.e., optic in bag and haptic in sulcus) may provide satisfactory anatomical outcome (Fig. 6) [12].

Surgical Outcomes

Temporary cessation of ocular growth is reported after adequate IOP control in eyes with AL > 22 mm and in children aged 3 months or older [13].

Our experience with 31 eyes of primary congenital glaucoma (post trabeculectomy) with visually significant cataract undergoing lens aspiration surgery showed a mean best corrected visual acuity of 6/60 (Snellen's) at 1 year postoperatively. Reasonably predictable refractive results were obtained in these eyes, provided glaucoma was well controlled [14].

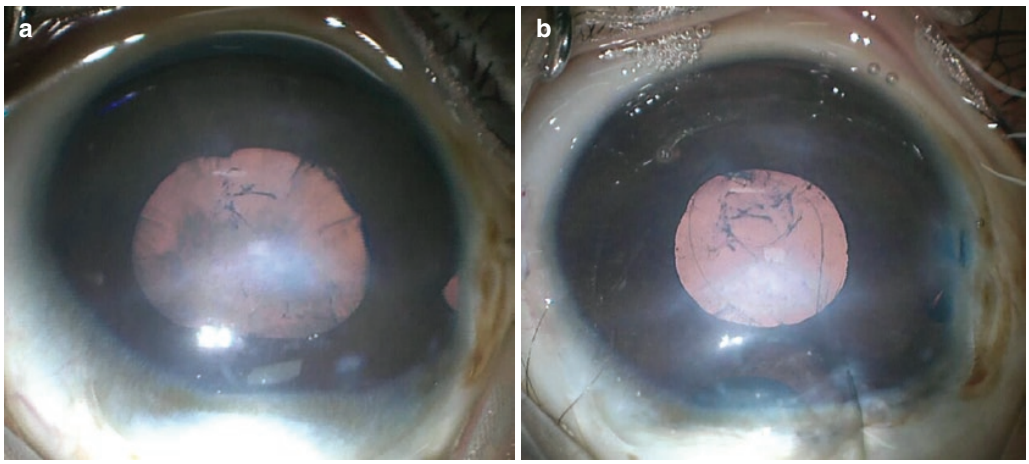

Fig. 6: Fifteen-month-old child with congenital glaucoma with corneal haze with Haab striae and large cornea (buphthalmos). (**a**) Preoperative picture with Anterior and posterior subcapsular cataract. (**b**) Postoperative picture with IOL in sulcus with optic capture with anterior and posterior capsulorhexis (bag complex) for better centration.

Thus, besides control of IOP, visual rehabilitation of buphthalmic eyes may involve appropriate management for amblyopia, keratoplasty for corneal opacity in addition to timely cataract surgery for visually significant cataract. Buphthalmic eyes undergoing cataract surgery can achieve successful refractive and visual outcomes if careful preoperative planning is carried out regarding the choice of IOL type and IOL power, taking into consideration the adequacy of intraocular pressure control, accurate biometry, assessment of bag size and use of appropriate IOL power formulae.

Anterior Segment Dysgenesis

Anterior segment dysgenesis (ASD) is a group of disorders arising from abnormal development in cornea, iris, lens and angle structures. This includes Axenfeld's anomaly, Rieger's anomaly, Axenfeld-Rieger syndrome (ARS), Peters anomaly, sclerocornea, aniridia, posterior keratoconus, and iridogoniodysgenesis. It occurs due to abnormalities in neural crest differentiation and migration. Various classifications are used for describing ASD depending either on their clinical features or area of involvement [15-17]. Lens abnormalities are not uncommon in cases with ASD. Townsend, Font, and Zimmerman have classified ASD based on involvement as Descemet layer defect alone or associated with lens abnormalities or with iris stromal abnormalities. This involvement of lens suggested the effects of primary mesenchymal defect on the development of lens [17].

Embryology

The surface ectoderm invaginates and forms lens vesicle in the embryonic cup at sixth week of gestation. Then, neural-crest-derived tissue migrates in three waves beneath this surface ectoderm. The surface ectoderm forms the corneal epithelium. The three waves forms endothelium,

corneal stroma, and iris stroma. Any arrest in the development of these layers may affect further development of anterior chamber leading to different presentations of ASD [18].

Genetics

Many genes are involved in the ASD with variable degree of penetrance. Forty percent cases occur due to involvement of PITX2 (4q25) and FOXC1 (6p25). Typically, PITX2 disruption is associated with ARS with ocular and dental abnormalities, and FOXC1 is associated with ARS with hearing or cardiac abnormalities. Others associated with ARS include PAX6 (11p13) and FOXO1A (13q14) [19, 20]. ARS has autosomal dominant inheritance pattern in 70% cases. In Peter's anomaly, rare cases have been attributed to PITX2, FOXC1, and PAX6 mutations, but the majority of cases are sporadic [21-23].

Clinical Features

- Axenfeld-Rieger syndrome
- Axenfeld anomaly presents as posterior embryotoxon (Fig. 7) (anteriorly displaced Schwalbe line) and iris strands adhered to the anteriorly displaced Schwalbe line. Rieger anomaly includes posterior embryotoxon, pseudopolycoria, and iris atrophy (Fig. 8) while Rieger syndrome is Rieger anomaly along with systemic findings including facial bone defects, hypertelorism, telecanthus, maxillary hypoplasia, dental abnormalities (microdontia and hypodontia), umbilical abnormalities or pituitary involvement. Thus, they are now considered as a spectrum of disorder termed as Axenfeld-Rieger syndrome (Fig. 9). It may vary from subtle changes in the angle to severe ocular changes. Systemic involvement may also include cardiac and endocrine system. Fifty percent cases with ARS are associated with glaucoma [24, 25].

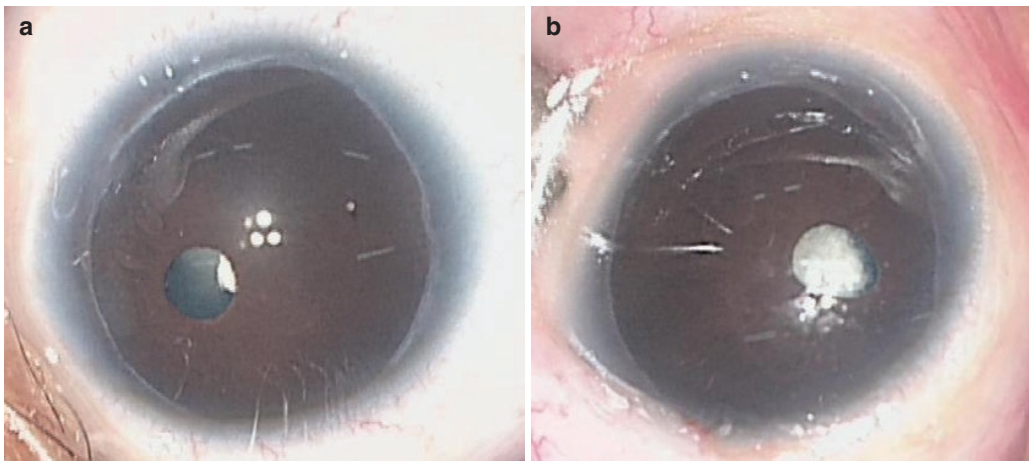

Fig. 7: Mild variant of Axenfield-Rieger syndrome (**a, b**) Posterior embryotoxon in 9-month-old child with cataract in right and left eye, respectively. Also notice presence of corectopia in both eyes.

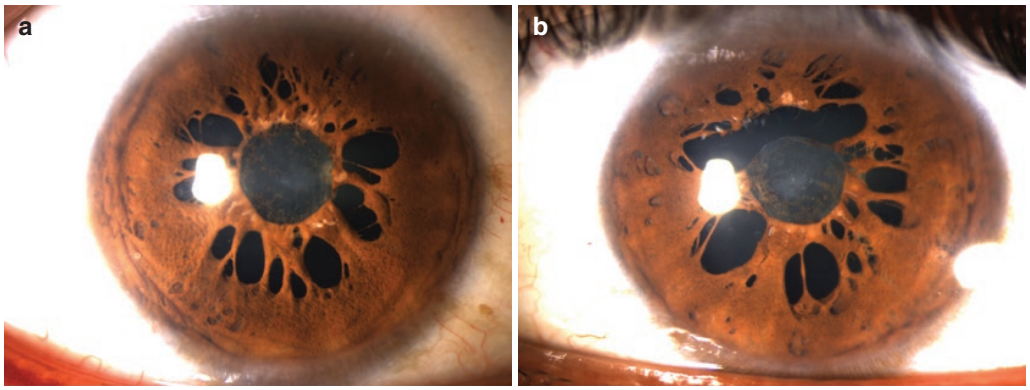

Fig. 8: (**a, b**) Rieger Anomaly-polycoria and iris atrophy in 7-year-old girl in right and left eye respectively.

Fig. 9: Severe variant of Axenfeld-Rieger syndrome—posterior embryotoxon with corectopia, iris atrophy and polycoria along with total cataract.

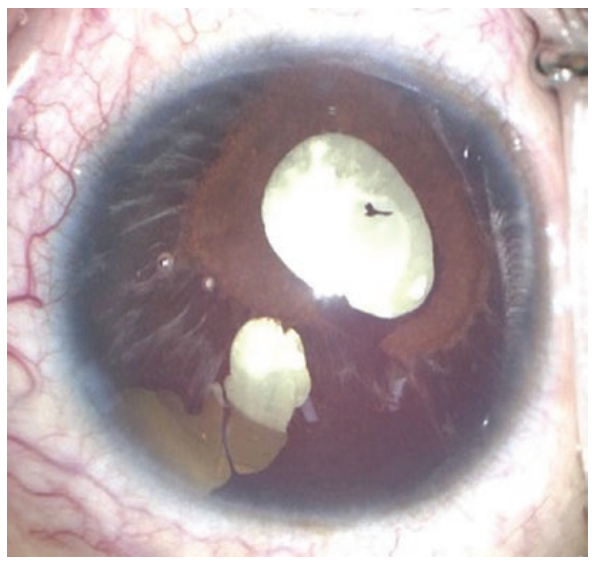

- Peters anomaly
- Peter syndrome is characterized by a shallow anterior chamber, synechiae between iris and cornea and central corneal opacity. It occurs due to defect in endothelium, Descemet membrane and posterior stroma due to the defect in the migration of the neural crest cells. This syndrome can vary in severity with ocular findings ranging from unilateral mild central corneal opacity to severe bilateral microphthalmia, corneal opacification, cataract, and glaucoma. Eighty percent of cases have bilateral presentation. The Peters anomaly has been further divided into type I and type II. Type I Peters anomaly is categorized by central corneal opacity and iridocorneal adhesions (Fig. 10). Type II Peters anomaly has a more severe phenotype with corneal opacity and lens involvement with iridocorneal touch with or without cataract (Fig. 11). The Peters plus syndrome includes the anterior segment findings with systemic

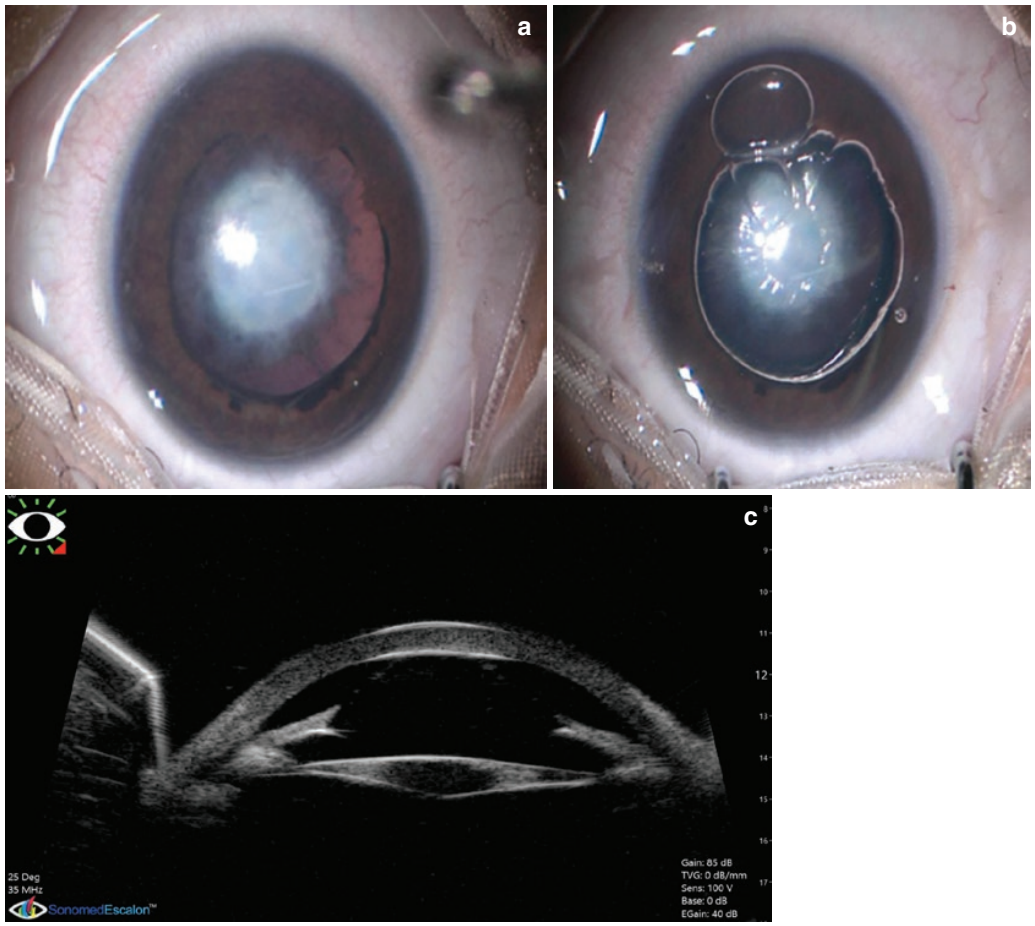

Fig. 10: Peter's anomaly type 1 in 2-month-old child. (**a**) Small corneal opacity with iridocorneal adhesions with cataract. (**b**) Intraoperative picture after ingestion of air in anterior chamber, irregular air bubble is seen due to iridocorneal adhesions. (**c**) Ultrasound biomicroscopy of the same showing fine central iridocorneal adhesions.

developmental anomalies. These include craniofacial dysmorphism, cleft lip/palate, short stature, brachydactylyl, ear abnormalities, and mental retardation [26, 27].

- Aniridia

  Aniridia is a rare congenital disorder characterized by iris hypoplasia along with other abnormalities of the eye [28]. Ocular abnormalities include dry eye, aniridia associated keratopathy (AAK) (Fig. 12), angle abnormalities, glaucoma, cataract, foveal hypoplasia, optic nerve hypoplasia, nystagmus, or strabismus [29-31]. Cataract morphology may be anterior or posterior subcapsular, lamellar, cortical, total or a combination of the above [28] (Fig. 13). Zonular weakness may be seen and ectopia lentis may be associated in some patients [28]. This can be managed with placement of capsular tension ring in mild cases (Fig. 14). Anterior polar or pyramidal cataract may be associated with aniridia along with remnants of persistent fetal vasculature [32] (Fig. 15).

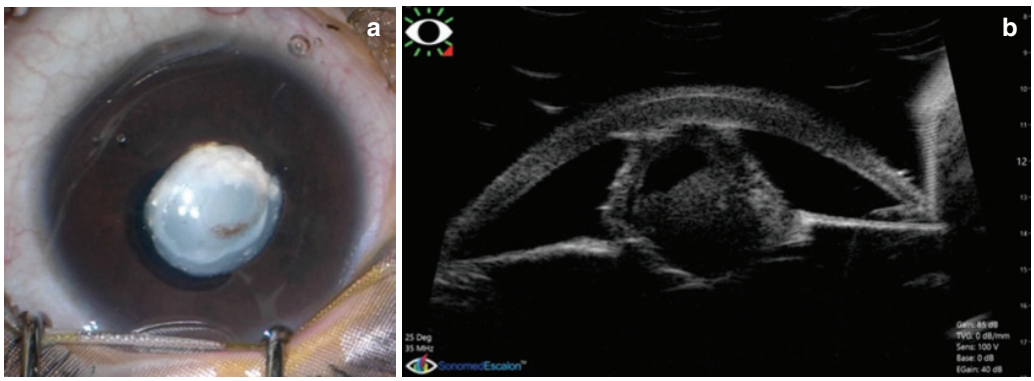

Fig. 11: Peter's anomaly type 2 in 4-month-old child. (**a**) Central corneal opacity with total cataract. (**b**) Ultrasound biomicroscopy of the same showing iridolenticular adhesions with anterior displacement of lens.

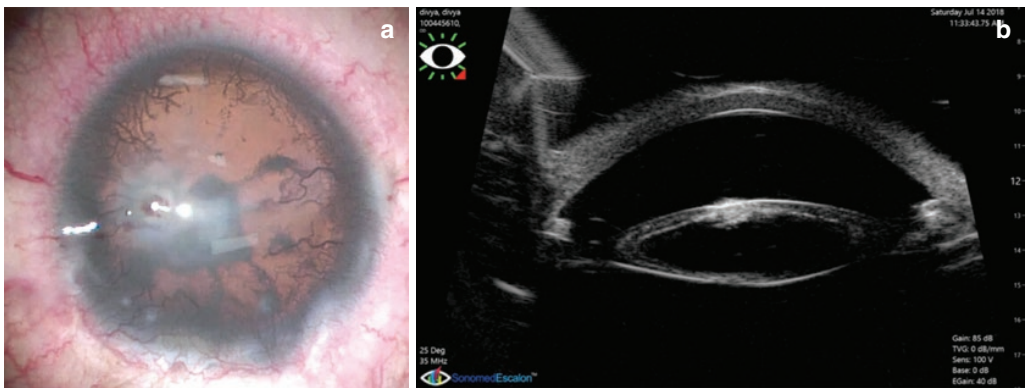

Fig. 12: Aniridia associated keratopathy with corneal opacity with 360° pannus. (**a**) Clinical picture. (**b**) Ultrasound biomicroscopy of the same showing anterior subcapsular cataract, not clearly seen clinically.

Differential Diagnosis

The differential diagnosis of ASD includes obstetric trauma, congenital glaucoma, intrauterine infections like rubella, herpes simplex virus and bacterial infections, iridocorneo-endothelial syndrome (Fig. 16), metabolic diseases like mucopolysaccharidosis, mucolipidoses and tyrosinosis, congenital hereditary endothelial dystrophy, congenital hereditary stromal dystrophy and dermoids.

Investigations

Apart from usual investigations ultrasound biomicroscopy may allow us to preoperatively assess the area beneath the corneal opacity. It helps us to determine the area of corneal opacity, depth of opacity, presence of iris adhesion, anterior chamber depth and angle details in the involved area. The lens can be visualized and observed for kerato-lenticular adhesion or presence of any tilting

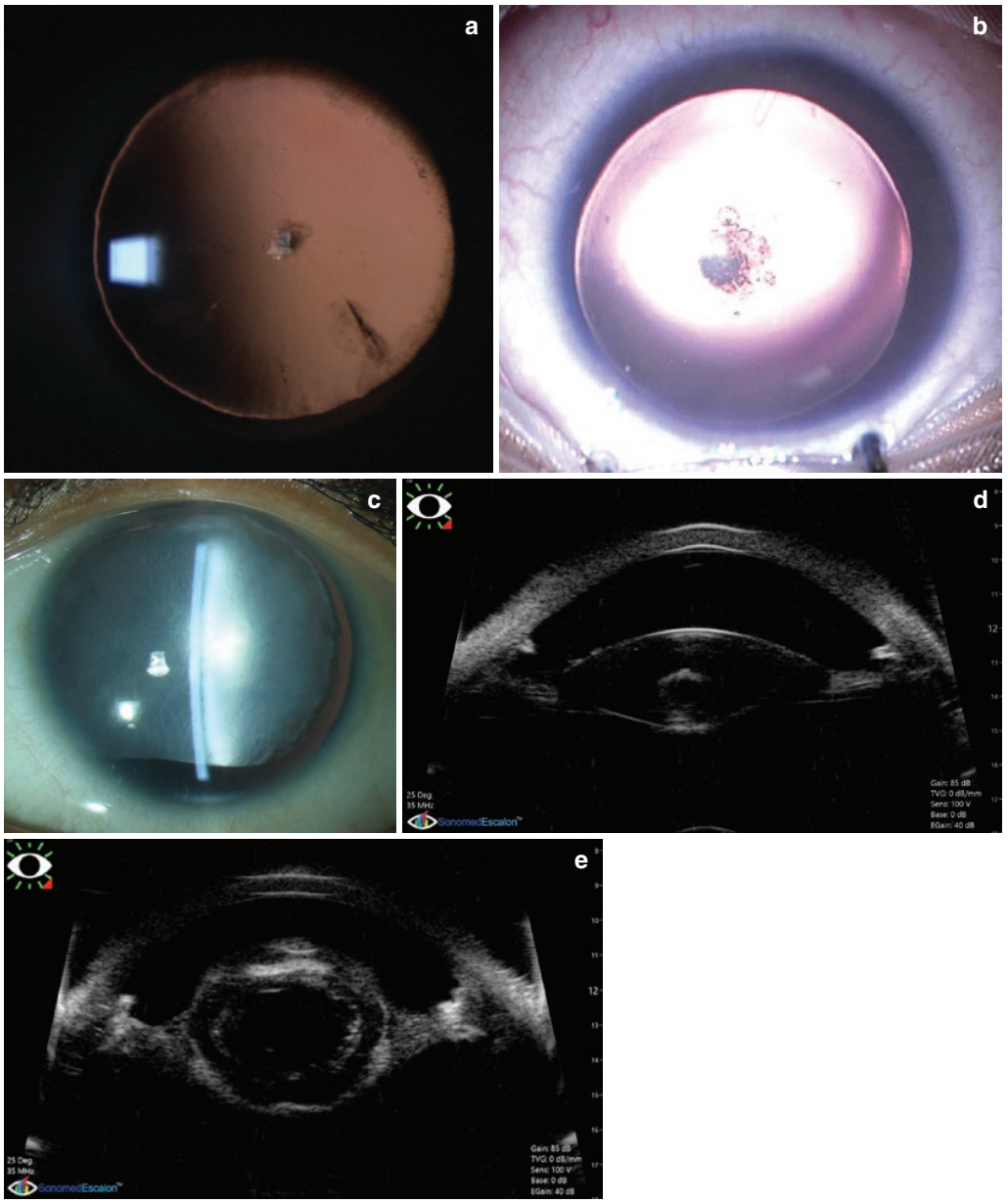

Fig. 13: Aniridia with cataract. (**a**) Clinical picture of insignificant anterior polar with cortical cataract. (**b**) Clinical picture of posterior subcapsular cataract. (**c**) Clinical picture of total cataract with inferior notching due to zonular laxity (Pseudo-coloboma). (**d**) UBM of aniridia patient showing minimal cataract and remnant of iris stump clearly with no subluxation. (**e**) UBM of aniridia patient with anterior polar and zonular cataract with zonular laxity causing increase in lens globularity.

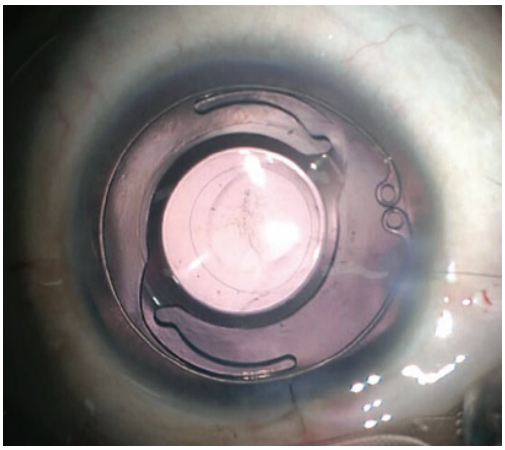

Fig. 14: Postoperative picture of aniridia with mild subluxation. Notice anterior and posterior capsulorhexis with well-centered IOL in bag with capsular tension ring.

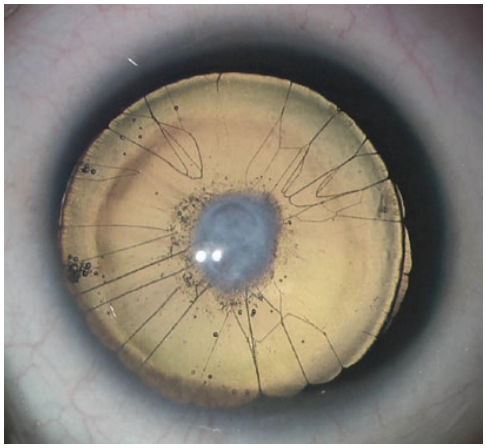

Fig. 15: Aniridia with anterior polar cataract with remnant of persistent fetal vasculature.

Fig. 16: Sixteen-year-old girl with Cogan Reese syndrome. Notice atophic iris and corectopia with iris nodules.

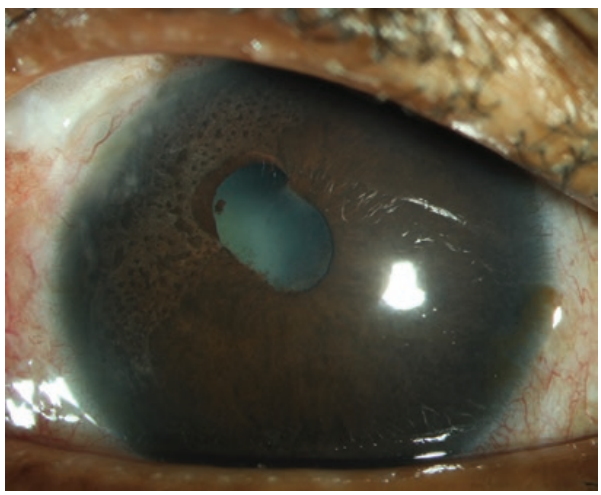

of the lens (Figs. 10b, 11b, and 13d, e). This can help us in the planning of the cataract surgery and a better outcome.

Surgical Pearls

Patients with ASD should be screened for glaucoma and managed appropriately. They require optimization of visual function which includes refractive error prescription and tinted contact lenses for photophobia. This is important for prevention and treatment of amblyopia. Few patients may also require surgery for corneal opacity, lens abnormality or glaucoma management. Various challenges may be involved in the cataract surgery in cases with ASD.

- Corneal abnormalities: Corneal opacity or AAK may cause difficulty in visualization. Staining of the anterior capsule enhances its visualization during capsulorhexis. Other methods like use of illumination techniques like transcorneal oblique illumination or endoscope assisted surgery can help in better visualization but are time-consuming methods with a greater learning curve [33-35]. Image-guided surgery using femtosecond laser for cataract surgery in peter syndrome has also been recently used [36]. However, the depth and height of the femtosecond laser should be cautiously adjusted to avoid damage to the endothelium.
- Presence of kerato-lenticular adhesion increases difficulty in surgical maneuvering. There may be risk of Descemet and endothelial damage during release of the keratolenticluar adhesions and difficulty to achieve appropriate size regular capsulorhexis. We have also noticed "irregular air bubble" in anterior chamber as a sign of presence of adhesions when they are not clearly visible (Fig. 17a, b).
- Iris abnormalities like corectopia, polycoria, iridocorneal adhesion, posterior synechiae between iris and lens may require anterior segment reconstruction may be required with synechiae release, anterior chamber formation or pupilloplasty along with the cataract surgery. Aniridia patients require use of tinted glasses or contact lens. Iris prosthetic devices may be used [37]. There is risk of secondary glaucoma, corneal decompenstion, band shaped keratopathy and device displacement [38] (Fig. 18).
- Zonular weakness: Aniridia cases have been reported with zonular laxity and lens subluxation. Use of capsular tension ring in cases with mild zonular laxity may give more desirable anatomical outcomes.
- Glaucoma management in cases with ASD is of importance and may include medical management, surgical management or both. Thus, a regular follow-up with monitoring of visual acuity and the intraocular pressure is crucial.

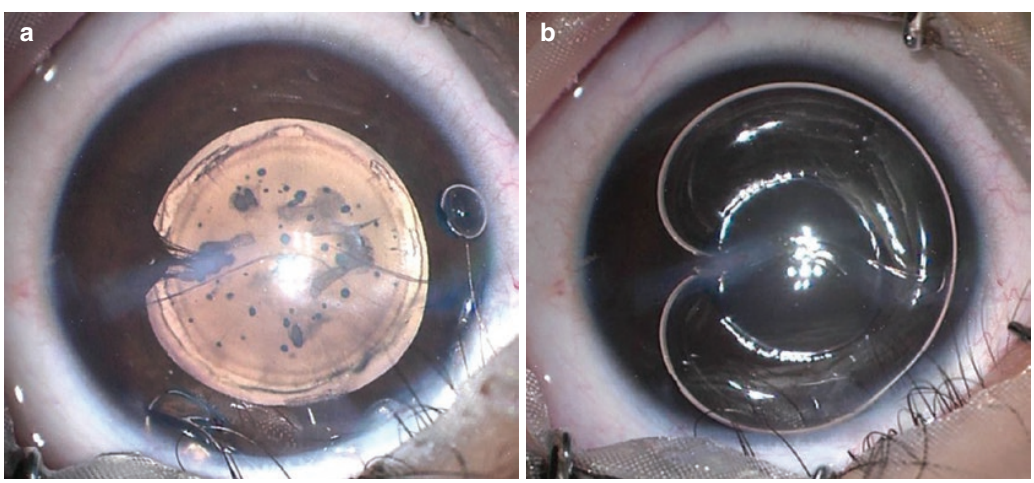

Fig. 17: Irregular air bubble sign in Anterior segment dysgenesis with glaucoma. (**a**) Corneal opacity with iridocorneal adhesions with Haab striae with anterior capsular pigments and zonular cataract. (**b**) Intraoperative picture after ingestion of air in anterior chamber, irregular air bubble is seen. Iridocorneal adhesions which were not clearly seen preoperatively are enhanced.

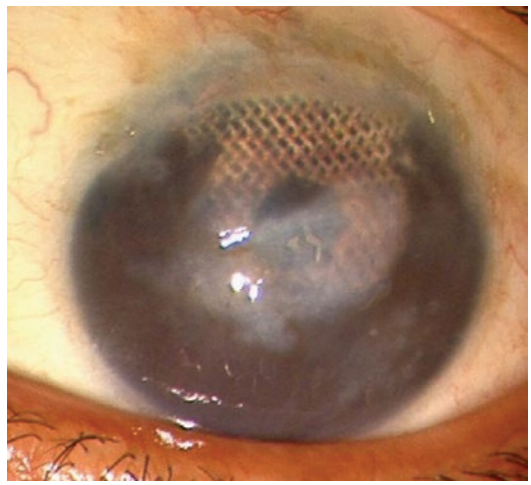

Fig. 18: One year postoperative picture of patient operated with Iris implant (outside center) with acquired aniridia (traumatic) with band shaped keratopathy and corneal decompensation.

Challenges in surgery in patients with ASD have to be carefully dealt with, in order to achieve satisfactory visual outcome. In addition to cataract surgery, glaucoma management is of utmost importance in these cases.

References

1. Wiggs JL, Damji KF, Haines JL, Pericak-Vance MA, Allingham RR. The distinction between juvenile and adult-onset primary open-angle glaucoma. Am J Hum Genet. 1996;58(1):243–4.
2. Feroze KB, Patel BC. Buphthalmos. In: StatPearls [Internet]. Treasure Island: StatPearls Publishing; 2018. http://www.ncbi.nlm.nih.gov/books/NBK430887/.
3. Yanoff M, Duker JS. Ophthalmology. 3rd ed. Philadelphia: Mosby Elsevier; 2009.
4. Basic and clinical science course (2011–2012). Glaucoma. American Academy of Ophthalmology.
5. Edmunds B, Thompson JR, Salmon J, Wornald RP. The national survey of trabeculectomy III. Early and late complications. Eye. 2002;16:297–303.
6. Adelman RA, Brauner SC, Afshari NA, Grosskreutz CL. Cataract formation after initial trabeculectomy in young patients. Ophthalmology. 2003;110:625–9.
7. Daugeliene L, Yamamoto T, Kitazawa Y. Cataract development after trabeculectomy with mitomycin C: a 1-year study. Jpn J Ophthalmol. 2000;44:52–7.
8. Khokhar SK, Pillay G, Agarwal E, Mahabir M. Innovations in pediatric cataract surgery. Indian J Ophthalmol. 2017;65(3):210–6.
9. Hugkulstone CE. Changes in keratometry following trabeculectomy. Br J Ophthalmol. 1991;75(4):217–8.
10. Chan HHL, Kong YXG. Glaucoma surgery and induced astigmatism: a systematic review. Eye Vis [Internet]. 2017;4. https://www.ncbi.nlm.nih.gov/pmc/articles/PMC5691392/.
11. Vaz FM, Osher RH. Cataract surgery and anterior megalophthalmos: custom intraocular lens and special considerations. J Cataract Refract Surg. 2007;33(12):2147–50.
12. Sukhija J, Kaur S, Pandav SS, Kaushik S, Raj S, Ram J. Cataract surgery in children with buphthalmos. Clin Experiment Ophthalmol. 2016;44(8):739–40.
13. Dietlein TS, Jacobi PC, Krieglstein GK. [Eyeball growth after successful glaucoma surgery in the 1st year of life--follow-up values for primary congenital glaucoma]. Klin Monbl Augenheilkd. 1998;213(2):67–70.
14. Khokhar S, Yadav D, Gupta S, Chaurasia AK, Gupta A, Gupta V. Refractive outcomes of cataract surgery in primary congenital glaucoma. Eye (Lond). 2018; https://doi.org/10.1038/s41433-018-0253-6.
15. Waring GO, Rodrigues MM, Laibson PR. Anterior chamber cleavage syndrome. A stepladder classification. Surv Ophthalmol. 1975;20:3–27.

16. Shields MB, Buckley E, Klintworth GK, Thresher R. Axenfeld-Rieger syndrome. A spectrum of developmental disorders. Surv Ophthalmol. 1985;29:387–409.
17. Townsend WM, Font RL, Zimmerman LE. Congenital corneal leukomas. 2. Histopathologic findings in 19 eyes with central defect in Descemet's membrane. Am J Ophthalmol. 1974;77:192–206.
18. Beauchamp G, Knepper P. Role of the neural crest in anterior segment development and disease. J Pediatr Ophthalmol Strabismus. 1984;21:209–14.
19. Glaser T, Walton DS, Maas RL. Genomic structure, evolutionary conservation and aniridia mutations in the human PAX6 gene. Nat Genet. 1992;2:232–9.
20. Phillips JC, *et al*. A second locus for Rieger syndrome maps to chromosome 13q14. Am J Hum Genet. 1996;59:613–9.
21. Dahl E, Koseki H, Balling R. Pax genes and organogenesis. Bioessays. 1997;19:755–65.
22. Doward W, Perveen R, Lloyd IC, Ridgway AE, Wilson L, Black GC. A mutation in the RIEG1 gene associated with Peters' anomaly. J Med Genet. 1999;36(2):152–5. PMID: 10051017; PMCID: PMC1734311.
23. Iseri SU, *et al*. Seeing clearly: the dominant and recessive nature of FOXE3 in eye developmental anomalies. Hum Mutat. 2009;30:1378–86.
24. Fitch N, Kaback M. The Axenfeld syndrome and the Rieger syndrome. J Med Genet. 1978;15:30–4.
25. Chang TC, Summers CG, Schimmenti LA, Grajewski AL. Axenfeld-Rieger syndrome: new perspectives. Br J Ophthalmol. 2012;96:318–22.
26. Bhandari R, Ferri S, Whittaker B, Liu M, Lazzaro DR. Peters anomaly: review of the literature. Cornea. 2011;30: 939–44.
27. Harissi-Dagher M, Colby K. Anterior segment dysgenesis: Peters anomaly and sclerocornea. Int Ophthalmol Clin. 2008;48:35–42.
28. Nelson LB, Spaeth GL, Nowinski TS, Margo CE, Jackson L. Aniridia. A review. Surv Ophthalmol. 1984;28:621–42.
29. Eden U, Riise R, Tornqvist K. Corneal involvement in congenital aniridia. Cornea. 2010;29:1096–102.
30. Chang JW, Kim JH, Kim SJ, Yu YS. Congenital aniridia: long-term clinical course, visual outcome, and prognostic factors. Korean J Ophthalmol. 2010;28:479–85.
31. Singh B, Mohamed A, Chaurasia S, Ramappa M, Mandal AK, Jalali S, Sangwan VS. Clinical manifestations of congenital aniridia. J Pediatr Ophthalmol Strabismus. 2014;51:59–62.
32. Khokhar S, Sinha G, Sharma R, Patil B, Mahabir M, Nayak B. Anterior pyramidal cataract: a rare association. JAMA Ophthalmol. 2015;133(4):e144626. https://doi.org/10.1001/jamaophthalmol.2014.4626.
33. Farjo AA, Meyer RF, Farjo QA. Phacoemulsification in eyes with corneal opacification. J Cataract Refract Surg. 2003;29:242–5.
34. Moore JE, Herath GD, Sharma A. Continuous curvilinear capsulorhexis with use of an endoscope. J Cataract Refract Surg. 2004;30:960–3.
35. Al Sabti K, Raizada S, Al Abduljalil T. Cataract surgery assisted by anterior endoscopy. Br J Ophthalmol. 2009;93:531–4.
36. Hou JH, Crispim J, Cortina MS, Cruz Jde L. Image-guided femtosecond laser-assisted cataract surgery in Peters anomaly type 2. J Cataract Refract Surg. 2015;41(11):2353–7. https://doi.org/10.1016/j.jcrs.2015.10.045. PMID: 26703482.
37. Srinivasan S, Ting DS, Snyder ME, Prasad S, Koch HR. Prosthetic iris devices. Can J Ophthalmol. 2014;49(1):6–17.
38. Mostafa YS, Osman AA, Hassanein DH, Zeid AM, Sherif AM. Iris reconstruction using artificial iris prosthesis for management of aniridia. Eur J Ophthalmol. 2018;28(1):103–7.

Source: Dhull C., Khokhar S.K. (2022) Congenital Glaucoma and Anterior Segment Dysgenesis. In: Khokhar S.K., Dhull C. (eds) Essentials of Pediatric Cataract Surgery. Springer, Singapore. https://doi.org/10.1007/978-981-16-0212-2_15.

CLINICAL VIGNETTE

A Case of Chronic Retinal Necrosis After Tube Shunt Surgery for Secondary Glaucoma Associated with Cytomegalovirus Corneal Endotheliitis

Katsue Imamachi[1*], Aika Tsutsui[1], Kaoru Manabe[2], Masaki Tanito[1]

Abstract

Background: We report a case of chronic retinal necrosis (CRN) combined with cytomegalovirus (CMV) corneal endotheliitis.
Case Presentation: An 80-year old man was diagnosed with CRN that developed after tube shunt surgery with vitrectomy for secondary glaucoma associated with CMV corneal endotheliitis. After the use of oral valganciclovir and panretinal photocoagulation, the retinal lesion resolved rapidly and he has maintained visual acuity better than before the onset of CRN.
Conclusions: Use of oral valganciclovir, prophylactic panretinal photocoagulation for the non-perfusion area and vitrectomy were effective in maintaining the visual acuity for the patient with CRN.

Keywords: Chronic retinal necrosis, Cytomegalovirus corneal endotheliitis, Polymerase chain reaction, Tube shunt surgery, Case report

Background

CRN, a new disease that was first described in 2013, is a slowly progressive occlusive vasculitis and granular retinitis in immunocompetent hosts. Its association with CMV-related inflammation is suspected [1]. We present a case of CRN that developed after implantation of an Ahmed Glaucoma Valve (New World Medical, Rancho Cucamonga, CA) with vitrectomy for secondary glaucoma associated with CMV corneal endotheliitis. Most previous cases of CRN had poor visual outcomes due to the complications, our case maintained visual acuity better than before the onset of CRN after the use of oral valganciclovir and prophylactic panretinal photocoagulation for the non- perfusion area. CRN combined with CMV endotheliitis has not been reported previously.

*** Correspondence:** kimamariko@yahoo.co.jp
[1]Department of Ophthalmology, Shimane University Faculty of Medicine, 89-1 Enya-cho, Izumo, Shimane 693-8501, Japan
[2]Division of Ophthalmology, Matsue Red Cross Hospital, Matsue, Shimane, Japan

Case Presentation

Our case is an 80-year-old man referred to our hospital with iritis and poor intraocular pressure (IOP) control in his left eye (OS). At the initial visit, the best-corrected visual acuity (BCVA) was 1.2 in the right eye (OD) and 0.3 OS, and the IOPs were 13 and 58 mmHg, respectively. Other than anterior chamber inflammation (Fig. 1a) and glaucoma, the fundus was normal (Fig. 1b). The patient had an ocular history of small-incisional cataract surgery and intraocular lens implantation OS 1 year previously. Except for systemic hypertension, he had no systemic diseases associated with immune deficiency and his human immunodeficiency virus (HIV) testing result was negative. The diagnosis of CMV corneal endotheliitis OS was made based on the previously-reported diagnostic criteria [2]. Detection of 5.2×10^5 copies/ml CMV DNA in the aqueous humor from the affected eye by a polymerase chain reaction (PCR) assay and keratic precipitates like coin-shaped lesion were observed. Serum IgM of Herpes simplex virus (HSV), Varicella zoster virus (VZV), and CMV were negative, and these IgG titers were slightly elevated to 61.8, 13.0, and 15.8, respectively; the CMV antigenemia was negative. After starting the treatment (0.5% ganciclovir eyedrops 6 times/day and 0.1% betamethasone 4 times/day) with the previously reported regimen [3], the anterior-segment inflammation resolved (Fig. 1c). Because the IOP control was poor despite four ocular antihypertensive drugs, tube shunt surgery using the Ahmed Glaucoma Valve (Model FP-7) was implanted 1 month after the initial visit. To preserve the corneal endothelial cells, a tube was inserted into the vitreous cavity [4]; for this purpose, 25-gauge pars plana vitrectomy was performed intraoperatively. After the glaucoma surgery, the IOP decreased below 10 mmHg with continuous use of topical ganciclovir and betamethasone without ocular antihypertensive medications. At the follow-up visit 2 months postoperatively, although he was unaware of visual worsening, granular retinitis and occlusive vasculitis were observed OS (Fig. 1d). At this time, PCR identified 1.8×10^4 copies/ml CMV in the aqueous humor. CRN associated with CMV infection was suspected, and oral valganciclovir (1800 mg for 2 weeks and then 900 mg for 1 week) was started in addition to the topical ganciclovir and betamethasone. Since the non-perfusion area extended throughout the entire fundus (Fig. 1e), panretinal photocoagulation was performed simultaneously. After valganciclovir was started, the retinal lesions resolved rapidly (Fig. 1f). At the final visit 12 months after the diagnosis of CRN, the BCVA and IOP were 0.6 and 11 mmHg, respectively, and the number of corneal endothelial cells of 2031 cells/mm^2 before the tube shunt implantation in the vitreous was maintained 2038 cells/mm [2]. The inflammation did not recur in the anterior segment and fundus during the follow-up period with a maintenance dose of topical 0.5% ganciclovir 4 times/day and 0.1% fluorometholone 4 times/day. Iris or angle neovascularization was not seen during the follow-up period.

Discussion and Conclusions

In the current case, the fundus lesion developed after tube shunt glaucoma surgery combined with vitrectomy in the pseudophakic eye with CMV endotheliitis and iritis, and CMV DNA in the aqueous humor was detected by PCR assay before and after the onset of CRN. Thus, the procedure might have facilitated transition of CMV virus from the anterior segment to the fundus,

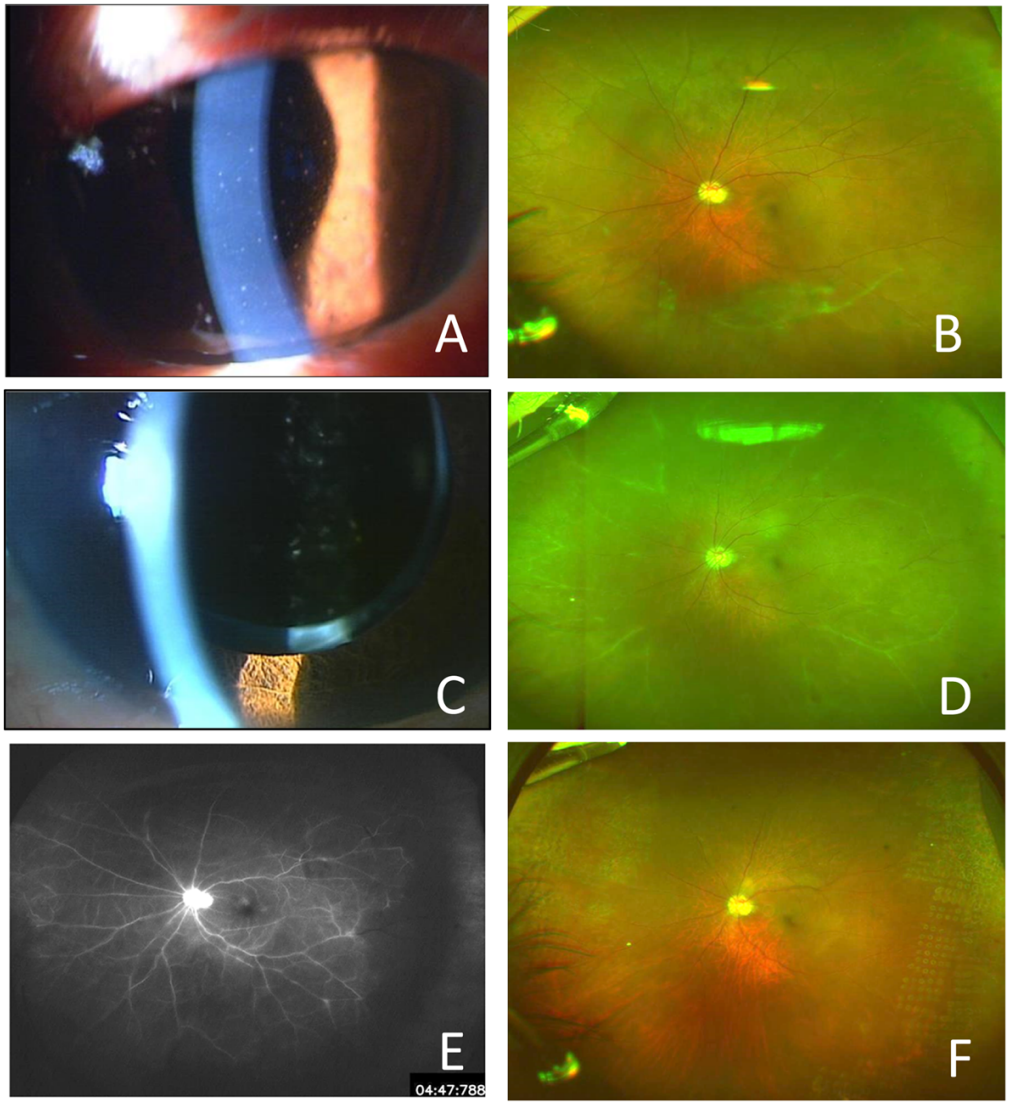

Fig. 1: Initial findings (**A, B**), after topical ganciclovir (**C**), at the onset of chronic retinal necrosis (**D, E**), and at the final visit (**F**). At the initial visit, slit-lamp examination shows keratic precipitates and anterior chamber cells in the left eye (OS) (**A**). A wide-field fundus camera photograph shows no retinitis or occlusive retinal vasculitis OS (**B**). Two weeks after the start of ganciclovir and steroid therapy, the iritis has resolved (**C**). Two months after the glaucoma surgery (3 months after the initial visit), occlusive vasculitis in the entire fundus and granular white lesions in the nasal fundus are seen OS (**D**); fluorescence angiography shows a non-perfusion area extending throughout the fundus (**E**). After combined therapy of oral ganciclovir for 3 weeks and panretinal photocoagulation, the occlusive vasculitis and granular retinitis have resolved (**F**).

although this speculation required to be proved. CRN combined with CMV endotheliitis has not been reported previously. To the best of our knowledge, three reports of seven CRN cases have been published [1, 5, 6]. In the initial report of five CRN cases [1], a retinal detachment developed

in one case and neovascular complications developed in four cases during the follow-up. Another case of CRN complicated by severe neovascular glaucoma was reported in Japan [5]. Although most previous cases had poor visual outcomes due to complications, our patient has maintained visual acuity more than before the onset of CRN. Use of oral valganciclovir, prophylactic panretinal photocoagulation and vitrectomy may explain the maintaining of visual acuity in the current case.

Abbreviations: CRN: Chronic Retinal Necrosis; CMV: Cytomegalovirus; IOP: Intraocular pressure; BCVA: Best-corrected visual acuity; HIV: Human immunodeficiency virus; PCR: Polymerase chain reaction

Acknowledgements: Not applicable.

Authors' contributions: KI drafted this manuscript and reviewed the literature. MT drafted and critically reviewed the manuscript. AT and KM collected the data. All authors read and approved the final manuscript.

Funding: Not applicable.

Availability of data and materials: All data generated during this study are included in this published article.

Declarations

Ethics approval and consent to participate: Not applicable.

Consent for publication: Written informed consent was obtained from the patient for publication of this case report.

Competing interests: The authors have no competing interests.

References

1. Schneider EW, Elner SG, van Kuijk FJ, Goldberg N, Lieberman RM, Eliott D, *et al*. Chronic retinal necrosis: cytomegalovirus necrotizing retinitis associated with panretinal vasculopathy in non-HIV patients. Retina. 2013;33(9):1791–9.
2. Koizumi N, Inatomi T, Suzuki T, Shiraishi A, *et al*. Clinical features and management of cytomegalovirus corneal endotheliitis: analysis of cases from the Japan corneal endotheliitis study. Br J Opthtalmol. 2015;99:54–8.
3. Fan N-W, Chung Y-C, Liu Y-C. Catherine Jui-Ling Liu, Yih-Shiuan Kuo, Pei-Yu Lin. Long-term topical ganciclovir and corticosteroids preserve corneal endothelial function in cytomegalovirus corneal endotheliitis. Cornea. 2016;35:596–601.
4. Chihara E, Umemoto M, Tanito M. Preservation of corneal endothelium after pars plana tube insertion of the Ahmed glaucoma valve. Jpn J Ophthalmol. 2012;56(2):119–27.
5. Matsuoka T, Asao K, Hashida N, Nishida K. Chronic retinal necrosis severely complicated by neovascular glaucoma: a case report. Case Rep Ophthalmol. 2017;8(3):489–95.
6. Weinlander E, Wubben TJ, Johnson MW. Subacute vision loss in a patient with limited immune dysfunction. JAMA Ophthalmol. 2020;138(2):208–9.

Source: Imamachi, K., Tsutsui, A., Manabe, K. *et al*. A case of chronic retinal necrosis after tube shunt surgery for secondary glaucoma associated with cytomegalovirus corneal endotheliitis. *BMC Ophthalmol* 21, 257 (2021). https://doi.org/10.1186/s12886-021-02019-w.

Postoperative Complicated Peripheral Cortical Cataract After Ultrasound Cycloplasty: A Case Report

Jihan Luo[1], Zhen Liu[2*], Lin Zhao[1], Yi Zhou[2], Li Kong[2], Yang Sun[2]

Abstract

Background: Ultrasound cycloplasty (UCP) is a non-invasive procedure for glaucoma treatment. Using high-intensity focused ultrasound to work on the ciliary body, the generation of aqueous humor can be reduced and the drainage of aqueous humor through the uveoscleral pathway can be enhanced. Recently, this therapy is gradually gaining clinical recognition. We report a case of a patient with glaucoma who accepted UCP in another hospital, but because of a worsening of a preexistent cataract and an insufficient IOP lowering effect, finally underwent cataract surgery in both eyes in our hospital, during the surgery we observed the unusual opacities probably due to UCP mistreatment.

Case Presentation: Patient was diagnosed as chronic angle closure glaucoma and catacract, accepted UCP on both eyes in another hospital 4 months ago. After the UCP therapy, the pupil was vertical ellipse, the UCP didn't have a sufficient effect on IOP and forced us to do cataract surgery to lower IOP. During the cataract surgery, some unusual white opacities in the peripheral cortex with clear boundary were found. Inaccurate WtW measurement was the most likely cause of the injury, which resulted in the use of the small-size UCP probe and the downward movement of the UCP probe.

Conclusion: UCP should not be a first-line treatment in a patient with cataract and angle closure glaucoma, cataract extraction is a better choice. The appropriate case selection needs to be more strict and the preoperative indexes measurements need to be more accurate.

Keywords: Ultrasound cycloplasty, Complicated peripheral cortical cataract, Pupil deformation, Case report

***Correspondence:** 38021222@qq.com
[1]Department of Ophthalmology, Chongqing General Hospital, University of Chinese Academy of Science, CGH, UCAS, Chongqing, China.
[2]Chongqing Aier Eye Hospital, No.2, Huatang Road, Jiangbei District, Chongqing, China.

Background

The treatment of glaucoma via ciliodestruction by high-intensity focused ultrasound was originally developed by Lizzi and Coleman. In the late 1980s, Sonocare manufactured an FDA-approved instrument for this treatment [1]. Ultrasound cycloplasty (UCP) is a non-invasive procedure for glaucoma treatment. Using high-intensity focused ultrasound to work on the ciliary body, the generation of aqueous humor can be reduced and the drainage of aqueous humor through the uveoscleral pathway can be enhanced. Recently, this therapy is gradually gaining clinical recognition. However, its safety and efficacy on patients have not been confirmed in a large sample size. We report a case of a patient with glaucoma who accepted UCP in another hospital, but because of a worsening of a preexistent cataract and an insufficient IOP lowering effect, finally underwent cataract surgery in both eyes in our hospital, during the surgery we observed the unusual opacities probably due to UCP mistreatment.

Case Presentation

The patient is a 63-year-old male who was diagnosed with chronic angle-closure glaucoma and accepted UCP in another hospital on both eyes 4 months ago. We asked the hospital for the preoperative data of the patient. The visual acuity was 20/160 (OD) and 20/40 (OS), and the best-corrected visual acuity (BCVA) was preserved at 20/100 (OD) with + 0.50D/– 1.50D*10 and 20/25 (OS) with + 0.75D/– 1.50D*165. The patient presented with bilateral cataract (C2N2P1 OD, C2N2P1 OS) according to Lens Opacities Classification System III (LOCS III). The optic discs of both eyes were pale with C/D = 0.9 (OD) and C/D = 0.8 (OS), respectively. The ultrasound biomicroscope (UBM) data were as follows: The iris of both eyes was swollen and the anterior chambers were narrow. In the right eye, the vertical anterior chamber depth was 2.24 mm and the corresponding sulcus-to-sulcus distance was 12.11 mm, and the horizontal anterior chamber depth was 2.28 mm with the corresponding sulcus-to-sulcus distance of 11.80 mm. In the left eye, the vertical anterior chamber depth was 2.26 mm and the corresponding sulcus-to-sulcus distance was 11.98 mm, and the horizontal anterior chamber depth was 2.24 mm with the corresponding sulcus-to-sulcus distance of 11.90 mm. Visual field examination showed that the right eye had a tubular visual field and the left eye had a peripheral visual field defect. Under the situation of using three kinds of anti-glaucoma drugs (methazolamide, carteolol hydrochloride, and brinzolamide), the baseline intraocular pressure (IOP) was 30 mmHg (OD) and 31 mmHg (OS), respectively. The preoperative anterior segment image (Fig. 1) showed that pupils of both eyes were regular circular and the depth of the anterior chamber was normal. The preoperative UBM image (Fig. 2) presented that the anterior chamber angle of both eyes was closed, the lens position was normal without deviation, and the anterior capsule was smooth without adhesion.

After evaluation, the hospital decided that the patient was suitable for UCP. We, on the other hand, have reservations about the decision and will elaborate on our reasons in the discussion section. The parameters of the operation were as below: OD: white-to-white (WtW, measured by calipers, IOL-master and corneal topography) distance = 11.4 mm, axial length (AL) = 23.21 mm;

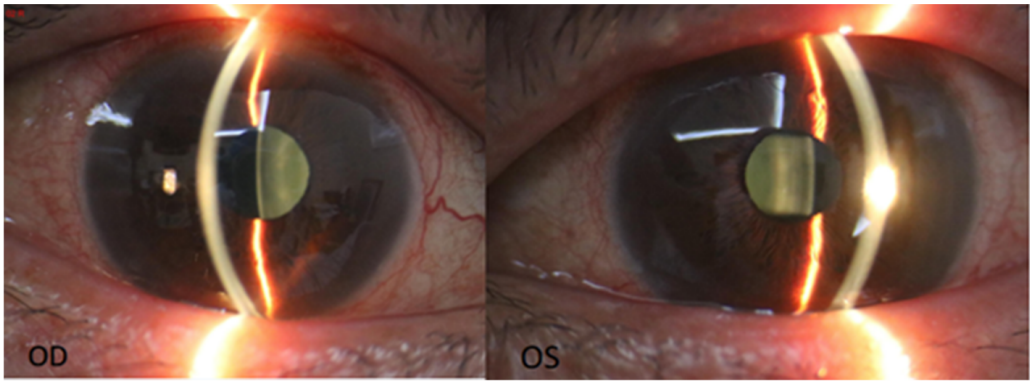

Fig. 1: Preoperative image of UCP: Both pupils are regular circular and the anterior chamber depth is normal.

OS: WtW distance = 11.4 mm, AL =23.03 mm. A high-intensity focused ultrasound (HIFU) equipment (EYE TECH CARE, sound glaucoma care, Version 3.20) was used for the UCP treatment. The parameters were as follows: Vacuum setpoint 225 mmHg; Duration 08.0 S; Pause 20.0 S; Probe Size 12 mm; Model T4T. SN = 18/172/018 / Unit = 15/007 (OD). SN = 18/172/013 / Unit = 15/007 (OS). UCP prepared for 10 sectors, but only 8 sectors treated (5 superior area/3 inferior area) on both eyes.

Three months after the UCP treatment, under the situation of using three kinds of anti-glaucoma drugs (methazolamide, carteolol hydrochloride, and brinzolamide), the IOP value of the patient fluctuated in the range of 22–30 mmHg and the visual acuity decreased to 20/250 (OD) and 20/80 (OS). It was found that the BCVA was preserved at 20/40 (OD) with −1.25 DC*35 and 20/32 (OS) with +2.50DS/−3.00 DC*155. After the UCP treatment, the image of the anterior segment (Fig. 3) exhibited that both pupils were vertical elliptical, of which the diameters were 3.0 mm*5.0 mm (OD) and 3.0 mm*4.0 mm (OS), respectively. Also, local iris atrophy on the subnasal of the left eye was observed. The central anterior chamber depth was about 2.5 corneal thickness (CT). The left eye had a peripheral anterior chamber depth of about 1/4 CT while the peripheral anterior chamber depth of the right eye varied greatly, which indicates an angle adhesion. The patient presented with bilateral cataract (C2N3P1 OD, C2N2P1 OS) according to LOCS III. The UBM image (Fig. 4) showed that both pupils were deformed, in which the left eye had an irregular superior suspensory ligament and the lens of the right eye deviated. The central anterior chamber depth was about 2.32 mm (OD) and 2.25 mm (OS), respectively. As shown in the image, the anterior chamber angle was closed in all directions while the ciliary body displaced forward to the root of the iris in both eyes. Both lenses showed enhanced echo. It is seen that there exists adhesion in the anterior capsule periphery of both lenses and the lens position of the right eye deviates.

Thus, we decided to perform cataract surgery on the right eye of the patient. Considering the lens position deviation and irregular suspensory ligament, we planned to implant a capsule tension ring into the eye to maintain the stability of the capsular bag. During the process of phacoemulsification, as Fig. 5 showed, several continuous localized white opacities in the peripheral

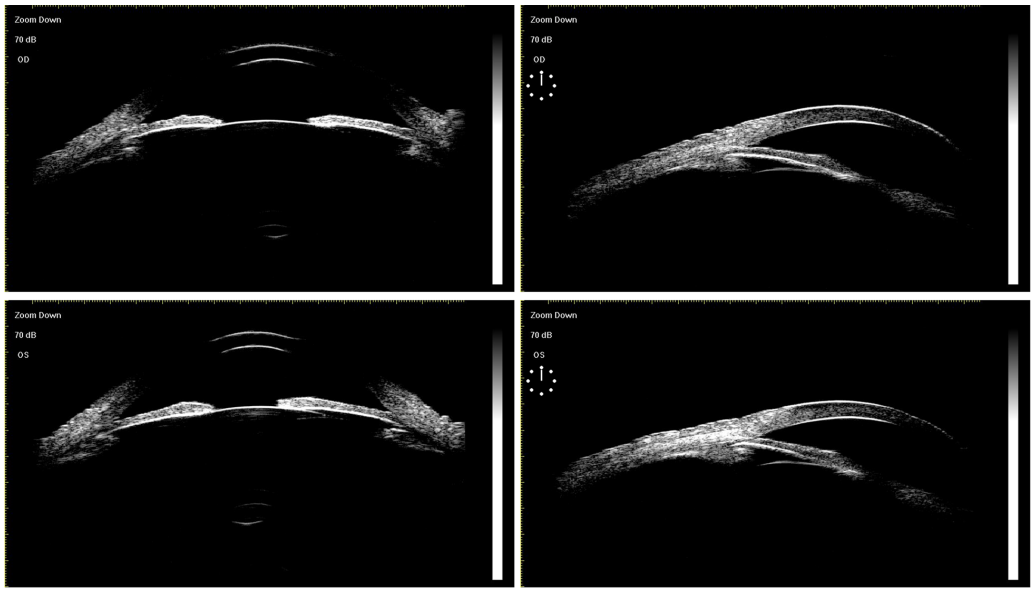

Fig. 2: Preoperative UBM image of UCP: Both eyes have anterior chamber angle closure, the lens position is normal without deviation, and the anterior capsule is smooth without adhesion.

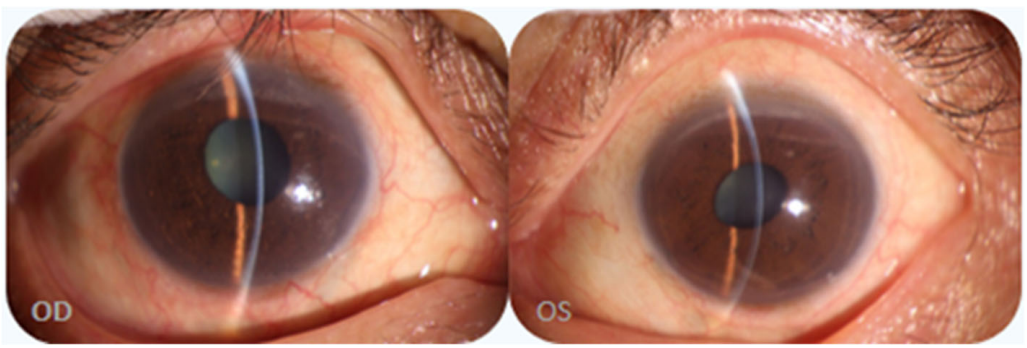

Fig. 3: Postoperative image of UCP: The diameters of two pupils were 3.0 mm*5.0 mm (OD) and 3.0 mm*4.0 mm (OS), respectively. Local iris atrophy on the subnasal of the left eye was observed. The central anterior chamber depth is about 2.5 corneal thickness (CT). The left eye had a peripheral anterior chamber depth of 1/4 CT while that of the right eye varied greatly, which indicates an angle adhesion.

cortex with clear boundaries were observed, which could not be found before the operation even if after mydriasis. Because the opacities were in the equator part of the lens, it could only be found when they were dragged out by I/A piece. At last, an intraocular lens was implanted into the eye. The 5-day postoperative visual acuity was 20/50, and the IOP value was 22 mmHg. After taking two anti-glaucoma drugs (carteolol hydrochloride and brinzolamide), the IOP value dropped to 8 mmHg 3 days later.

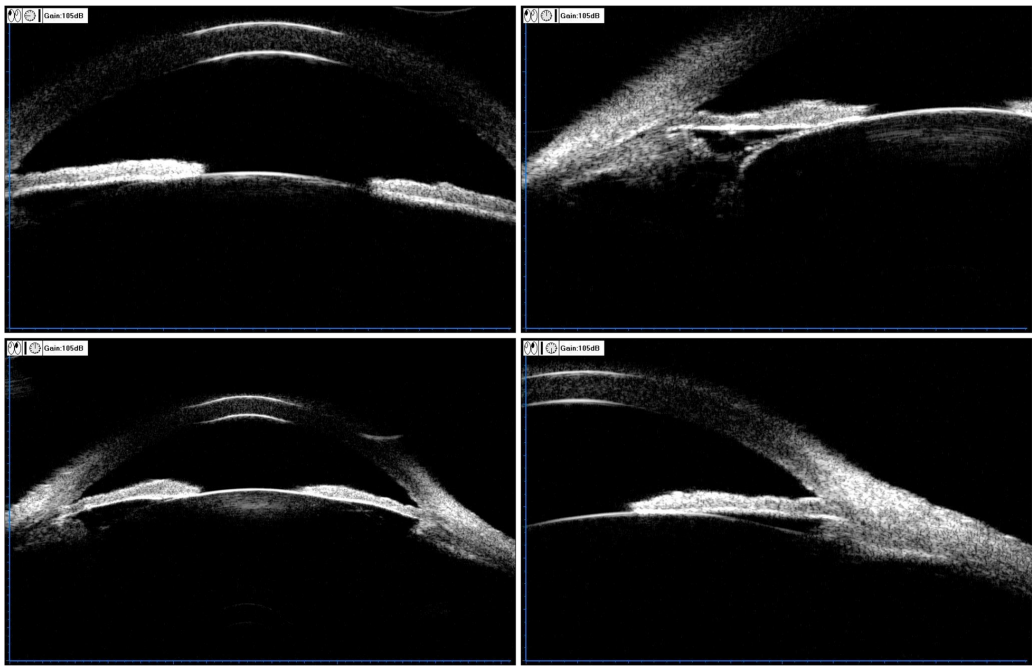

Fig. 4: Postoperative UBM image of UCP: The central anterior chamber depth is about 2.32 mm (OD) and 2.25 mm (OS), respectively. The anterior chamber angle was closed in all directions and the ciliary body displaced forward to the root of the iris in both eyes. The shape of the superior suspensory ligament is irregular in the left eye. Both lenses show enhanced echo. There exists an adhesion in the anterior capsule periphery in both lenses while the lens position of the right eye deviates.

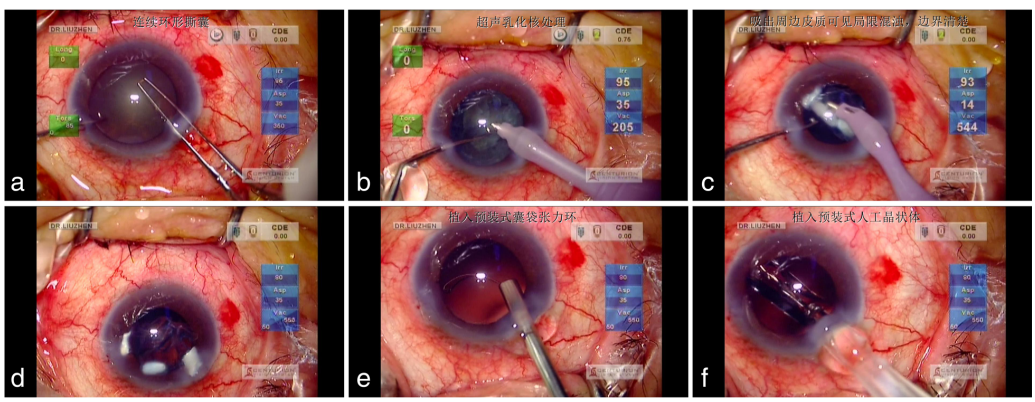

Fig. 5: Process of phacoemulsification: a Continuous curvilinear capsulorhexis; b Phacoemulsification; c In the process of phacoemulsification, several continuous localized white opacities with clear boundaries are found in the peripheral cortex; d The single image of the white opacities in the peripheral cortex; e A capsule tension ring is planted into the eye; f Intraocular lens implantation.

Five days after the surgery of the right eye, cataract surgery was taken on the left eye. It was also found in the process of I/A that there was a large white opacity formed by the fusion of several pieces of calcification in the equator part of the lens. As Fig. 6 showed, although the opacities in the right eye were four separated pieces while the opacity in the left eye was a whole piece, they were all white calcified plaques.

Discussion

Using a small computer-controlled eye probe to focus the high-intensity ultrasound energy on the ciliary body, UCP facilitates epithelium to generate aqueous humor in a non-incision, quantifiable, and accurate way. In general, the thermal effect of ultrasound is theoretically controllable within the submillimeter level. In this case, however, the continuous localized white opacities are so regular with markedly clear boundaries, which is neither any kind of natural cataract we know nor reported in any literature before. So it leads to a question that whether the ultrasound thermal injury causes the cataract. The location of those opacities is in the equator of the lens, where is just below the ciliary body. The shape of opacities also matches the effected area of ultrasound thermal damage according to some early research [2].

After the UCP treatment and cataract surgery, the IOP value of the patient still cannot reach an ideal level until the intervention of anti-glaucoma drugs. Therefore, we need to decide whether additional glaucoma surgery is necessary for the next step [3]. The pupil ovalization and accommodation loss and iatrogenic corneal astigmatism after UCP treatment also interfere with the visual acuity recovery of the patient in this case, which also has been reported by some other researches [4-6].

After careful retrospective analysis of the UCP procedure of this case, we reckoned that the inaccurate WtW measurement was the most likely cause of the injury, which might result in the use of the small-size UCP probe and the downward movement of the UCP probe during the surgery. Several papers [7-9] have proved that the WtW distance does not necessarily correspond

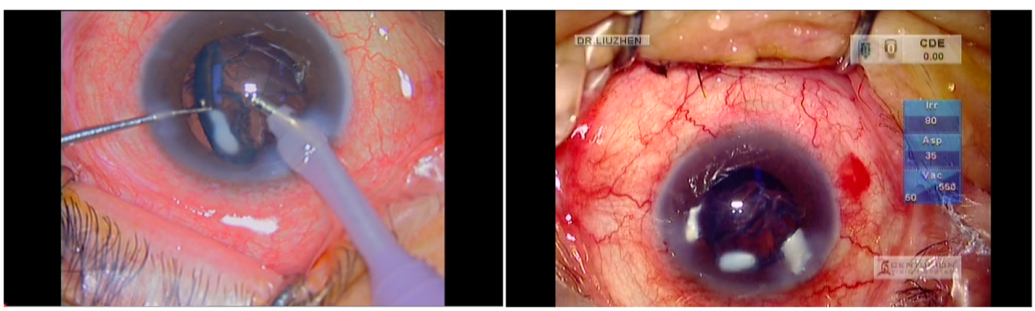

Fig. 6: Peripheral cortical cataract: Opacities were all located in the equator part of both lenses, which could not be seen by the shelter of pupils until they were dragged out. The opacities in the right eye were four separated pieces while the opacity of the left eye was a whole piece. The common thing is that they are all white calcified plaques.

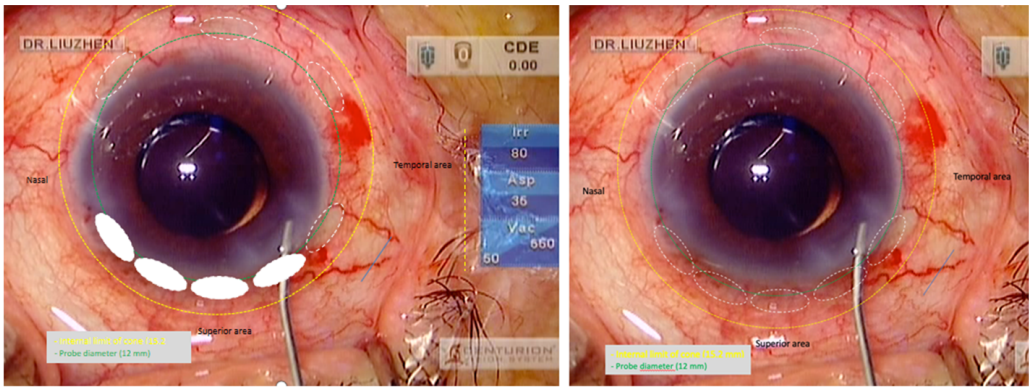

Fig. 7: Nonoptimal centering and optimal centering simulation (OD): The left figure illustrated a displacement of the probe and 4 lesions into the lens based on the 4 scleral marks (dotted line). The right figure showed the optimal centering simulation.

to the sulcus-to-sulcus distance using UMB and the former distance is an inaccurate indicator predicting the position of the ciliary processes. Figure 7 was a simulation of the nonoptimal centering and optimal centering (OD). The left figure illustrated a displacement of the probe and 4 lesions (full line) into the lens based on the 4 scleral marks (dotted line). The right figure showed the optimal centering simulation. Just because of the downward movement of the probe, the upper equatorial lens was injured by accident, forming a calcification with clear boundaries caused by ultrasonic thermal damage.

We are not sure whether such complicated peripheral cortical cataracts are frequent but lack of coverage due to concealment, or just an individual case of improper manipulation and improper selection of treatment patients. At least, however, in this case, we believe the best operation for this patient is cataract surgery rather than UCP. Cataract extraction is a well-accepted indication for angle-closure glaucoma, whereas UCP is a second-line treatment. In other words, if the patient is diagnosed with angle-closure glaucoma with cataract, we would choose cataract extraction as the first therapy.

According to the existing literature [10], indications for UCP include 1. Various refractory glaucomas such as primary open-angle glaucoma, primary angle-closure glaucoma, secondary glaucoma (for instance, neovascular glaucoma, secondary glaucoma after cataract surgery, glaucoma after corneal transplantation, etc.), and refractory glaucoma with uncontrolled intraocular pressure after multiple glaucoma surgeries; 2. No vision and no possibility of vision recovery; 3. No surgery opportunity and no surgery value; 4. Severe pain; 5. Poor general conditions that unable to tolerate surgery.

However, based on the complications this patient suffered, we believe that applying UCP treatment needs more caution and discretion. We should pay more attention to whether the

indications of UCP in the clinical application are too wide, or whether some other problems have been not observed or reported yet.

Conclusion

In this case, the UCP didn't have a sufficient effect on IOP and forced us to do cataract surgery to lower IOP. This lack of effect was due to the misplacement of the probe that caused the lens opacities. UCP should not be a first-line treatment in a patient with cataract and angle closure glaucoma, cataract extraction is a better choice. To maximize the efficacy of UCP and minimize the patients' loss, the appropriate case selection needs to be more strict and the preoperative indexes measurements need to be more accurate.

Abbreviations: UCP: Ultrasound cycloplasty; IOP: Intraocular pressure; BCVA: Best-corrected visual acuity; UBM: Ultrasound biomicroscope; CT: Corneal thickness; LOCS III: Lens Opacities Classification System III

Acknowledgements: Not applicable.

Authors' contributions: JHL and ZL contributed to the concept and study design. The patient was enrolled from LZ, LK, YS. The operation was performed by ZL. YZ collected the data. JHL made data interpretations and drafted the manuscript. All the authors including JHL, ZL, LZ, YZ, LK, YS were involved in the critical revision of the manuscript, supervision of the manuscript and final approval of the submission.

Funding: The authors have no financial sponsorship from any company or institution.

Availability of data and materials: The datasets generated and/or analysed during the current study are not publicly available due to an invasion of individual privacy but are available from the corresponding author on reasonable request.

Ethics approval and consent to participate: Not applicable.

Consent for publication: Written informed consent was obtained from the patient for publication of this case report and any accompanying images. A copy of the written consent is available for review by the Editor of this journal.

Competing interests: The authors declare that they have no competing interests.

References

1. Silverman RH, Vogelsang B, Rondeau MJ, Coleman DJ. Therapeutic ultrasound for the treatment of glaucoma [published correction appears in am J Ophthalmol 1991 Jul 15;112(1):105]. Am J Ophthalmol. 1991;111(3):327–37.
2. Lizzi FL, Packer AJ, Coleman DJ. Experimental cataract production by high frequency ultrasound. Ann Ophthalmol. 1978 Jul;10(7):934–42.
3. Giannaccare G, Vagge A, Sebastiani S, *et al*. Ultrasound Cyclo-Plasty in patients with Glaucoma: 1-year results from a multicentre prospective study. Ophthalmic Res. 2019;61(3):137–42.
4. Rivero-Santana A, Pérez-Silguero D, Pérez-Silguero MA, Encinas-Pisa P. Pupil Ovalization and accommodation loss after high-intensity focused ultrasound treatment for Glaucoma: a case report. J Curr Glaucoma Pract. 2019;13(2):77–8.
5. Sousa DC, Ferreira NP, Marques-Neves C, *et al*. High-intensity focused ultrasound Cycloplasty: analysis of pupil dynamics. J Curr Glaucoma Pract. 2018;12(3):102–6.

6. Marques RE, Sousa DC, Vandewalle E, *et al*. The effect of glaucoma treatment using high-intensity focused ultrasound on total and corneal astigmatism: a prospective multicentre study [published online ahead of print, 2020 May 18]. Acta Ophthalmol. 2020. https://doi.org/10.1111/aos.14467.
7. Oh J, Shin HH, Kim JH, Kim HM, Song JS. Direct measurement of the ciliary sulcus diameter by 35-megahertz ultrasound biomicroscopy. Ophthalmology. 2007;114(9):1685–8.
8. Kawamorita T, Uozato H, Kamiya K, Shimizu K. Relationship between ciliary sulcus diameter and anterior chamber diameter and corneal diameter. J Cataract Refract Surg. 2010 Apr;36(4):617–24.
9. Reinstein DZ, Archer TJ, Silverman RH, Rondeau MJ, Coleman DJ. Correlation of anterior chamber angle and ciliary sulcus diameters with white-to-white corneal diameter in high myopes using Artemis VHF digital ultrasound. J Refract Surg. 2009;25(2):185–94.
10. Posarelli C, Covello G, Bendinelli A, Fogagnolo P, Nardi M, Figus M. High-intensity focused ultrasound procedure: the rise of a new noninvasive glaucoma procedure and its possible future applications. Surv Ophthalmol. 2019;64(6):826–34.

Source: Luo, J., Liu, Z., Zhao, L. *et al*. Postoperative complicated peripheral cortical cataract after ultrasound cycloplasty: a case report. *BMC Ophthalmol* **21**, 16 (2021). https://doi.org/10.1186/s12886-020-01743-z. © The Author(s). 2021.

Notes:

SUN PHARMA

In Primary Open Angle Glaucoma & Ocular Hypertension

℞ BRIMOLOL

Brimonidine Tartrate 0.15% + Timolol Maleate 0.5%

For Combined Power, Greater Benefits...

PHMB EXHIBITS LOW TOXICITY[1,2]

- PHMB has broad spectrum anti-microbial activity with low toxicity
- PHMB can bind to & damage bacterial DNA
- 0.02% PHMB had minimal effect on the epithelial barrier function compared to BKC

1. Vontobel et al., J Clin Exp Ophthalmol 2015, 6:3
2. Bassam H Mashat, British Journal of Environmental Sciences Vol.4, No.1, pp.49-55, February 2016